

Multifunctional triazine-based nanoporous polymer as versatile organocatalyst for CO₂ utilization and C-C bond formation

Ruchi Sharma,¹ Ankushi Bansal,¹ C. N. Ramachandran² and Paritosh Mohanty^{1*}

¹*Functional Materials Laboratory, IIT Roorkee, Roorkee-247667, India*

²*Theoretical and Computational Chemistry Laboratory, Department of Chemistry, IIT Roorkee, Uttarakhand-247667, India*

E-mail: pmfcy@iitr.ac.in, paritosh75@gmail.com

Supporting information

1. General information	S2
2. Experiments	S3-5
3. Characterization of synthesised material	S6-15
4. Characterization of cyclic carbonates	S16-26
5. Theoretical calculation	S28
6. Characterization of methanol	S29-30
7. Table for Knoevenagel reaction	S32
8. Characterization of Knoevenagel products	S33-42

1. General information:

The FT-IR spectra of the MNENP was recorded on PerkinElmer Spectrum 2 FT-IR spectrophotometer in the wavelength range of 400-4000 cm^{-1} . Cross polarization magic angle spinning (CP-MAS) ^{13}C NMR spectrum of the MNENP was investigated by JEOL Resonance JNM-ECX-400II at 100 MHz for ^{13}C with MAS frequency of 10 kHz and 9000 scans. Chemical environment of the elements in MNENP was investigated by XPS (X-ray Photoelectron spectrometer, PHI-5000 VersaProbe III, ULVAC-PHI INC) and spectra was recorded using Al K_α as radiation source, at the analyzer pass energies of 280 eV for survey scan and 55 eV for high resolution scan of individual elements. The elemental analysis (C/H/N/S) was carried out using Thermo Flash 2000. The TGA/DTG analysis was performed at the temperature range of 25-900 $^\circ\text{C}$ with heating rate of 10 $^\circ\text{C min}^{-1}$ under Ar atmosphere on EXSTAR TG/DTA 6300. The XRD pattern was recorded on Rigaku ultima IV in 2θ range of 5-80 $^\circ$ using Cu K_α ($\lambda = 1.5405 \text{ \AA}$). The microstructure of MNENP was investigated using FE-SEM (Carl Zeiss Gemini 300) and TEM (TECNAI G²S-TWIN). The Brunauer Emmett Teller specific surface area (SA_{BET}) was estimated using the standard N_2 sorption analysis in Autosorb iQ2, Quantachrome instruments, USA. Prior to the analysis, the sample was degassed at 120 $^\circ\text{C}$ for 6 h. The pore volume was calculated at P/P_0 of 0.90 from the adsorption branch of the isotherm. The concentration of surface basic sites present in the MNENP catalyst was investigated by using CO_2 temperature programmed desorption (TPD) on a Micromeritics ChemiSorb 2750 instrument. For this, 66 mg of powdered sample was loaded inside a quartz U tube and degassed at 132 $^\circ\text{C}$ for 1 h in argon gas with a flow rate of 20 mL min^{-1} . After cooling to 80 $^\circ\text{C}$, the gas was changed to 99% CO_2 and treated at the same temperature for 1 h. The gas was switched over to helium at the same temperature and heated at 10 $^\circ\text{C min}^{-1}$ up to 750 $^\circ\text{C}$. The desorbed CO_2 quantification was monitored by using a thermal conductivity detector.

The investigation of the products formed using MNENP as organocatalyst was carried out by liquid state ^1H and ^{13}C NMR using JEOL RESONANCE ECX-400. The electrocatalytic studies were carried out in Autolab M204 (Metrohm) using 3 electrodes set-up. Purity of the products was investigated by gas chromatography (GC) (Perkin Elmer GC Clarus 680) & mass spectroscopy (MS) (Perkin Elmer MS Clarus SQ8T) and GC (Centurion Scientific CS5800).

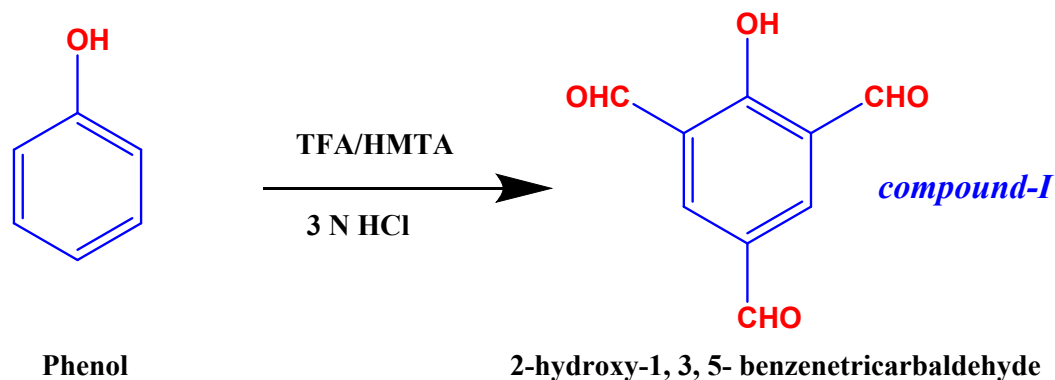
2. Experimental details

Materials:

Benzaldehyde (Himedia), malononitrile (Avra), hexamethylenetetramine (Lobachemie), hydrochloric acid (Merck), trifluoroacetic acid (SRL), methanol (Rankem), acetone (Rankem), dimethyl sulfoxide (DMSO) (Rankem), melamine (Lobachemie), phenol (Merck) and acetone (Avra) have been used as received without any further purification.

Synthesis of porous polymer (MNENP):

Synthesis of 2-hydroxy-1,3,5-benzenetricarbaldehyde (*compound-I*): In a typical synthesis, a mixture of 3.45 g of phenol, 35 ml of trifluoroacetic acid and 10 g of hexamethylenetetramine was heated at 120 °C for 20 h followed by 150 °C for 3 h, with continuous stirring. The reaction temperature was decreased to 120 °C and 50 ml of 3N HCl was added to it. The reaction temperature was further reduced to 100 °C and kept there for 30 min followed by cooling down to room temperature. A yellow color precipitate was formed which was filtered and washed several times with DI water and dried in vacuum oven at 60 °C. Yield: 3.1 g (54 %). The formation of the product, as shown in Scheme-S1, was confirmed by ¹H and ¹³C NMR, Fig. S1.^{S1}



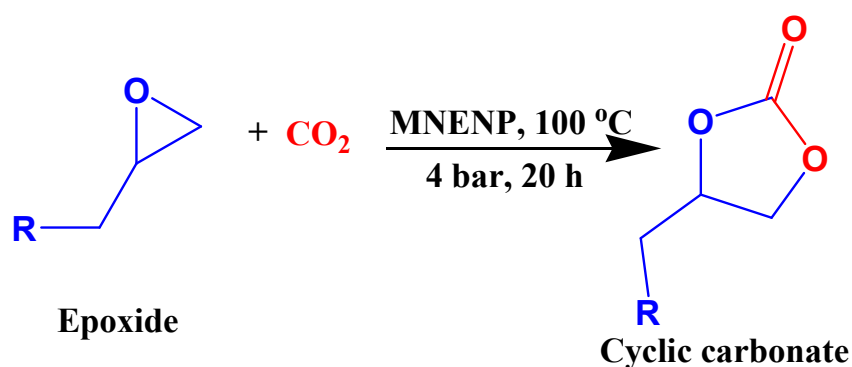
Scheme S1. Reaction scheme for the synthesis of 2-hydroxy-1,3,5-benzenetricarbaldehyde (*compound-I*).

Synthesis of nanoporous polymer (MNENP): For the synthesis of the desired polymeric material by condensing *compound-I* with melamine is given as follows. 1 mmol each of *compound-I* and melamine were dissolved in 20 ml of DMSO. The solution was heated at 170 °C for 24 h. An off-white coloured precipitate was formed which was filtered and washed with copious amount of water and methanol. To remove any trapped DMSO, the powder was refluxed in methanol for 24 h followed by drying in oven at 60 °C. The final product was designated as MNENP (Fig. 1a). In order to investigate the effect of reaction time and

temperature on the product formation and control of the textural properties, identical experiments were carried out for 12, 24 and 48 h at 170 °C and further at temperatures of 130, 150 and 180 °C for 24 h keeping all other experimental conditions same.

MNENP as metal-free organocatalyst for CO₂ utilization: The synthesized MNENP has been used in various pathways for the catalytic conversion of CO₂ as follow:

Reaction of CO₂ with epoxides to form cyclic carbonates: Catalytic amount (10 mg) of MNENP was used for the reaction of 0.25 ml of epoxide with CO₂ at a pressure of 4 bar in a high pressure reactor. The reactor was heated at 100 °C for 20 h (Scheme S2). After the completion of reaction, catalyst was separated by centrifugation and further washed with ethyl acetate 2-3 times. Final products were purified using column chromatography and analysed by ¹³C and ¹H NMR spectroscopy. The purity of the products was investigated using GC-MS.

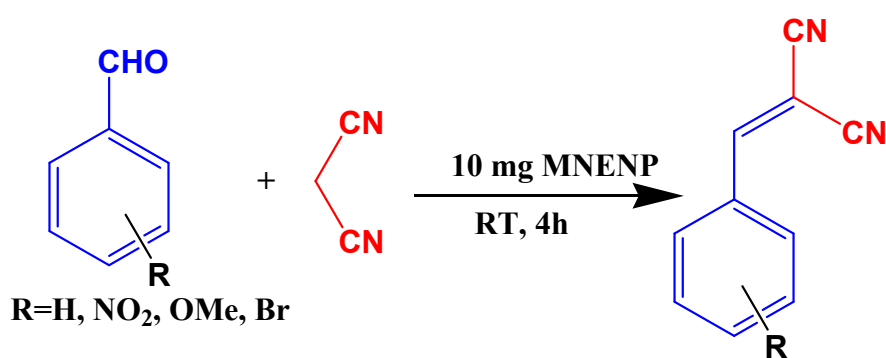


Scheme S2. Reaction scheme for the synthesis of Cyclic carbonate.

Electrocatalytic conversion of CO₂ to methanol: The electrocatalytic conversion of CO₂ was carried out using the MNENP as the active electrode material and the experiments were performed using a three-electrode set up in a gas-tight two-compartment electrolysis cell equipped with a KCl-saturated Ag/AgCl reference electrode and a platinum counter electrode as shown in Fig. S4. Typically, the MNENP based working electrode has been prepared by the following steps. Initially, PVDF is dissolved in NMP and to it, the mixture of MNENP and activated carbon which were homogeneously mixed prior to the addition, was dispersed. A slurry was formed after stirring for 24 h, which was painted onto a piece of graphite sheet of dimension 1×1 cm². The ratio of various components (PVDF, carbon black and MNENP) in the slurry is 1.5:1.5:7. The net active mass loading (MNENP) in the prepared electrode was 0.74 mg cm⁻². The electrolyte used in all these experiments was 400 ml of an aqueous 0.1 M KHCO₃ solution saturated with CO₂ (99.999% purity). The *pH* of the electrolyte solution changes from 8.65 to 6.89 in the saturated solution. The cyclic voltammetry (CV) studies was

carried out in the potential range from 0 to -2 V (vs. Ag/AgCl) at a scan rate of 5 mV s^{-1} . During electrolysis, CO_2 flow rate was of 20 ml min^{-1} to ensure continuous CO_2 saturation. Similar experiment was repeated with blank graphite sheet.

Knoevenagel Condensation: In a typical catalytic reaction via Knoevenagel condensation, 1 mmol of aromatic aldehyde and 1 mmol of malononitrile were condensed with 5 ml of methanol in the presence of 10 mg of MNENP at room temperature, Scheme 5. The progress of the reaction was monitored using TLC and complete conversion was obtained after stirring for 4 h at RT. The catalytic C-C bond formation was confirmed by 1H and ^{13}C NMR spectral analysis.



Scheme S3. Reaction scheme for Knoevenagel Condensation.

3. Characterization of synthesised material

NMR data of *Compound-I*:

^1H NMR (DMSO- D_6): 10.31 (s, 2H); 10.00 (s, 1H); 8.53 (s, 2H); 10.30 (s, 2H); 9.99 (s, 1H); 8.52 (s, 2H); ^{13}C NMR (DMSO- D_6): 191.91, 191.06, 166.16, 137.54, 128.48, 124.33 ppm as previously reported.^{S1}

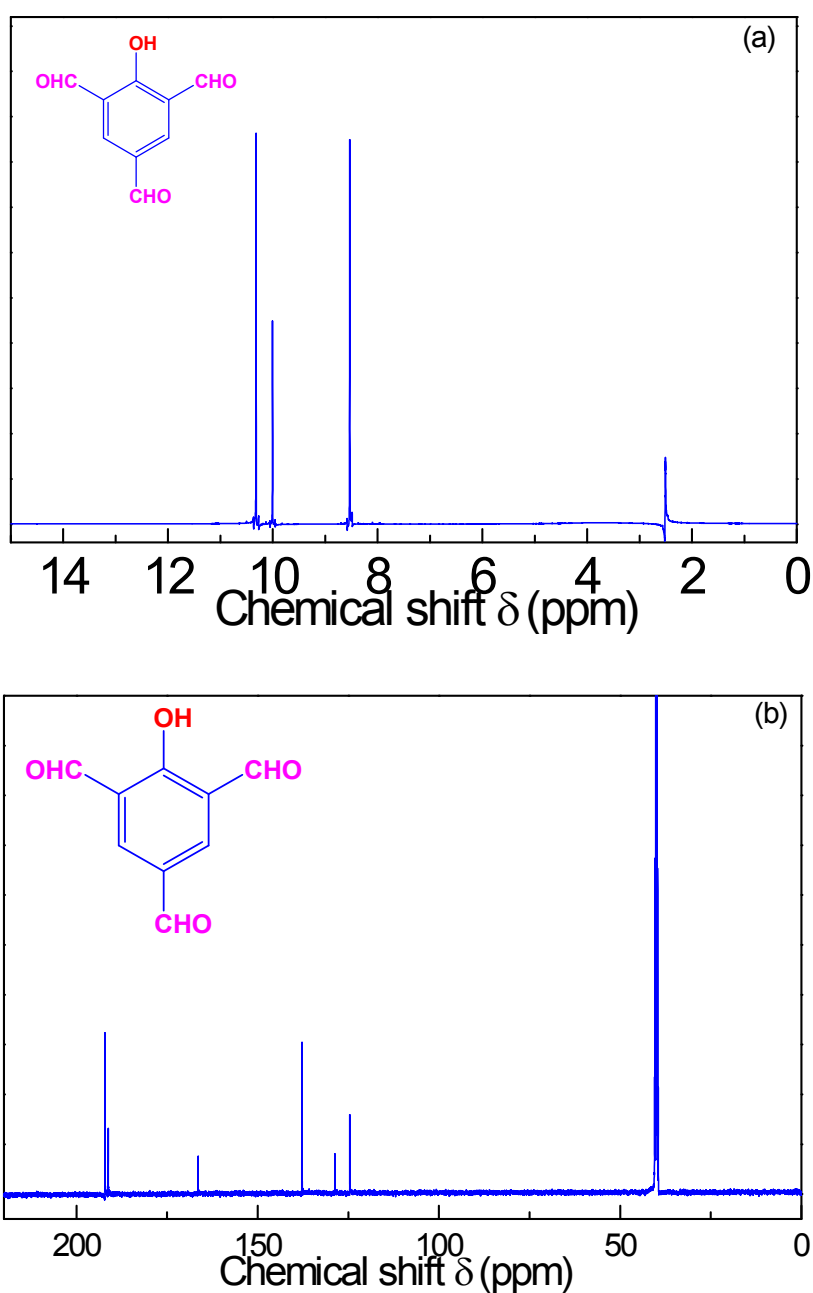


Fig. S1. (a) ^1H NMR (b) ^{13}C NMR spectra of *Compound-I* (2-hydroxy-1,3,5-benzenetricarbaldehyde).

Table S1. Description of FT-IR bands of MNENP synthesized by condensation of *compound-I* with melamine.

Bands	Bands Assignment
3445	N-H and -OH stretching
2955	Aliphatic C-H stretching
1645	C-N stretching of triazine ring
1548	C-N stretching of 2° amine
1480	Aromatic ring C=C stretching
1387	C-N-C stretching
1354	C-N stretching of CH-N
1200	C-OH stretching
1047	N-C-N stretching of methylene linkages
890	ring deformation, (N-H, C-H)
811	Aromatic C-H deformation
775	C-H deformation

NMR analysis of MNENP

The signal at 166 ppm (1) is attributed to the carbon of triazine moiety present in MNENP.^{S2a} For comparison, the ¹³C NMR of the precursors *compound-I* and melamine are given in the Fig. S1b and Fig. S2. It can be seen that the triazine carbon of the MNENP is observed at a minor up-field compared to the triazine carbon (168 ppm) of melamine. The resonance signal of the carbon of aromatic ring attached to the -OH group is observed at 157 ppm (2). A signal at 57 ppm (3) is due to tertiary carbon further supports the formation of amination linkage.^{S2b} The signals at 135, 128 and 122 are originated due to the (4), (5) and (6) carbon of aromatic ring as shown in the Fig. S1b. The absence of the signals of carbonyl carbon at ~192 and 191 ppm further support the complete condensation of *compound-I* with melamine.

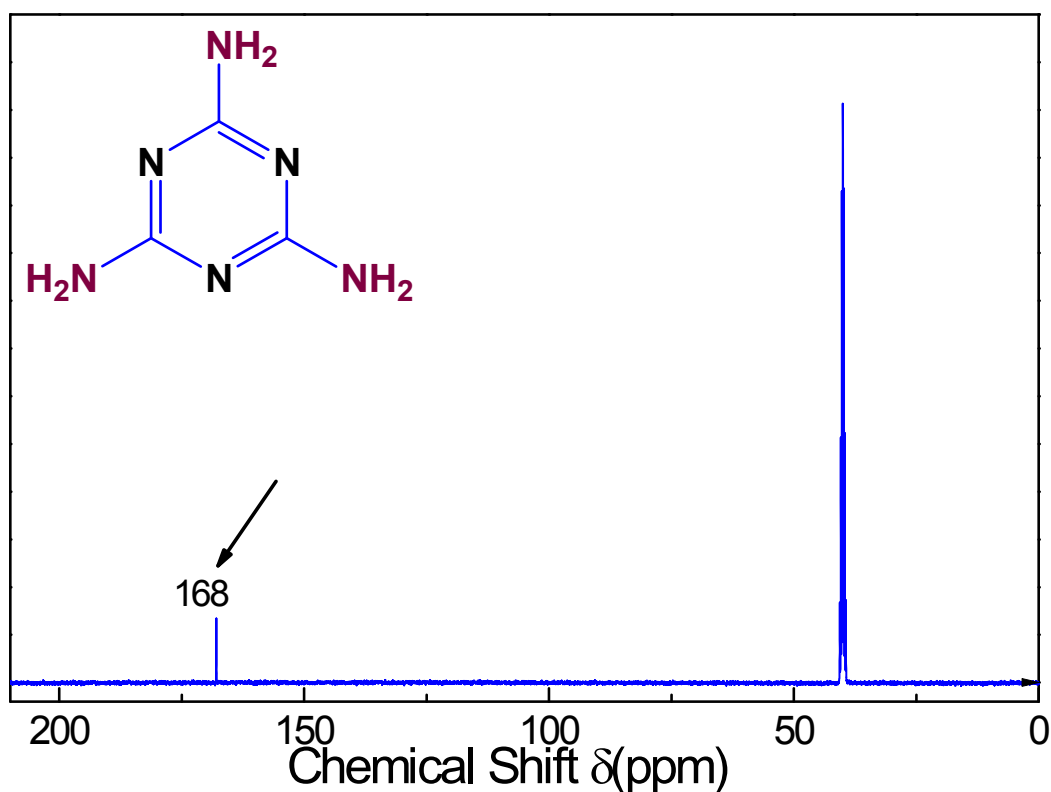


Fig. S2. ¹³C NMR spectra of Melamine.

XPS analysis of MNENP

The high resolution C1s spectrum in Fig. S3a has shown five different types of carbon present in the sample. The peak at 284.8 eV is attributed to the graphitic carbon originated from the carbon tape used for the sample mounting.^{S2a} The triazine carbon is observed at 287.4 eV. Two different types of aromatic carbons are observed at 285.1 and 286.4 eV. The peak at 288.5 eV is attributed to the carbon attached to the hydroxyl group. Unlike the ¹³C CP-MAS NMR where four different carbons are observed, XPS could not differentiate between these aromatic carbons due to a very minor change in the chemical environment. The N1s XPS (Fig. S3b) shows two peaks at 399.6 and 400.1 eV attributed to the -C=N- and -NH- functionalities, respectively.^{S2a,3} The O1s (Fig. S3c) spectrum has the maxima at 531.49 eV due to -OH functionality attached to the aromatic ring. A minor peak at 532.64 eV could be attributed to the -S=O from the trapped DMSO.^{S2a}

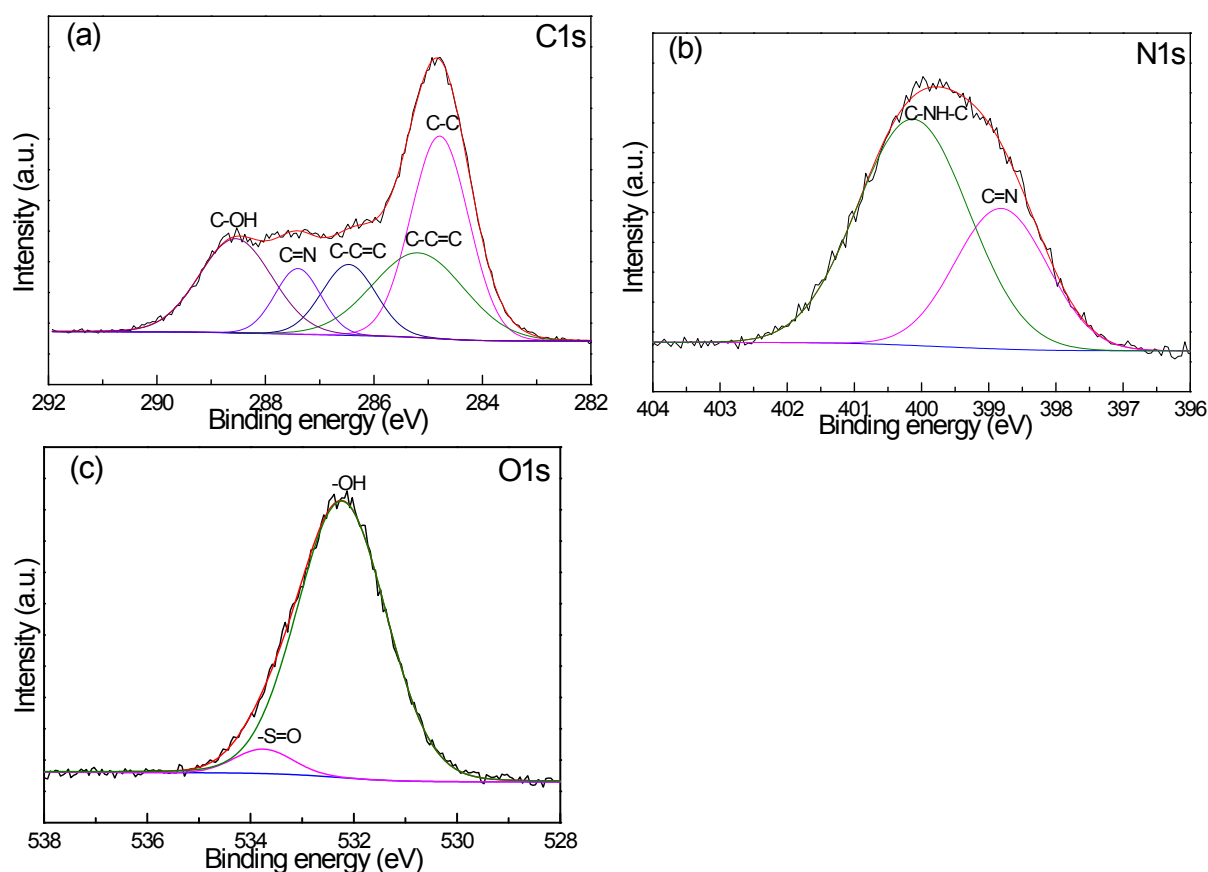


Fig. S3. (a) High-resolution C1s XPS spectrum, (b) High-resolution N1s XPS spectrum and (c) High-resolution O1s XPS spectrum of MNENP.

Electrocatalytic conversion of CO₂ into value added products

For electrocatalytic conversion of CO₂ into methanol, we have used a two-compartment electrochemical setup separated by proton exchange membrane (Nafion 211) as shown in Fig. S4.

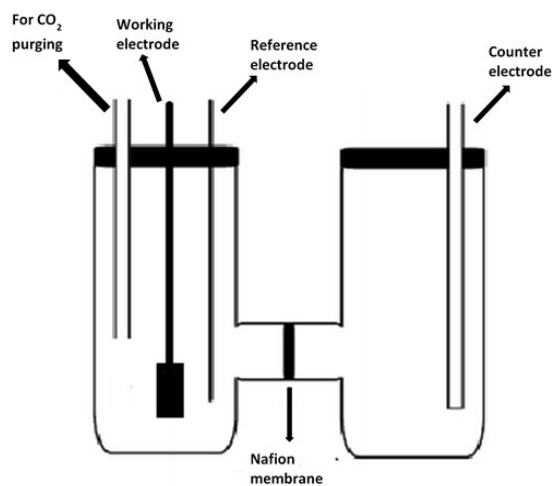


Fig. S4. Two compartment electrochemical setup separated by proton exchange membrane (Nafion 211).

Thermogravimetric analysis

TGA/DTG analysis was carried out under argon atmosphere to investigate the thermal stability of MNENP as shown in Fig. S5. The TGA/DTG thermograms shows multistep mass loss. The initial weight loss below 100 °C is due to the removal of adsorbed gases and trapped solvent/moisture. The second weight loss between 130 to 220 °C could be attributed to the removal of trapped DMSO from the MNENP framework. The presence of trapped DMSO in the specimen was also observed from the NMR and XPS investigations. The third and major weight loss above 300 °C could be attributed to the condensation and carbonization of the framework followed by the gradual decomposition of the material in a continuous manner.

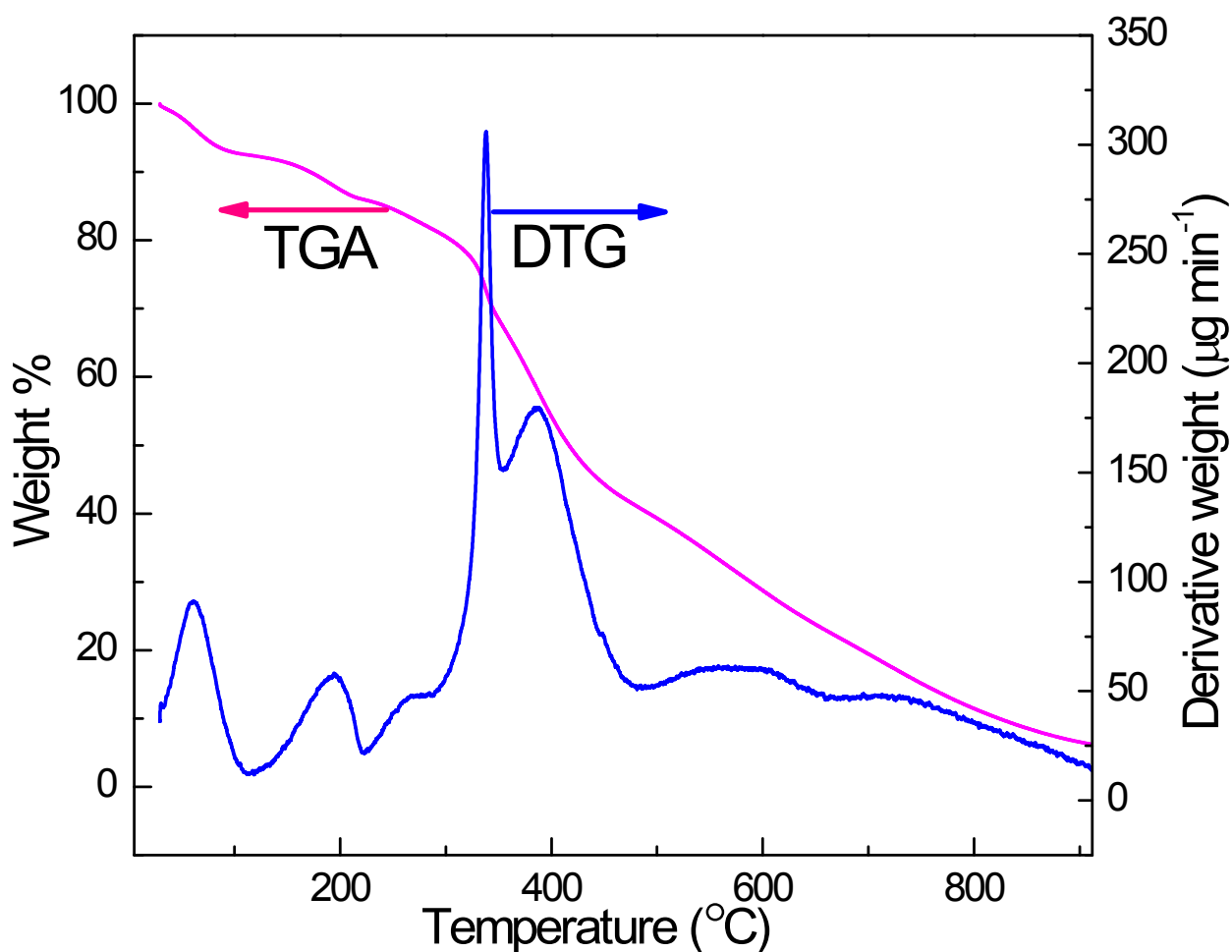


Fig. S5. Thermogravimetric analysis of MNENP.

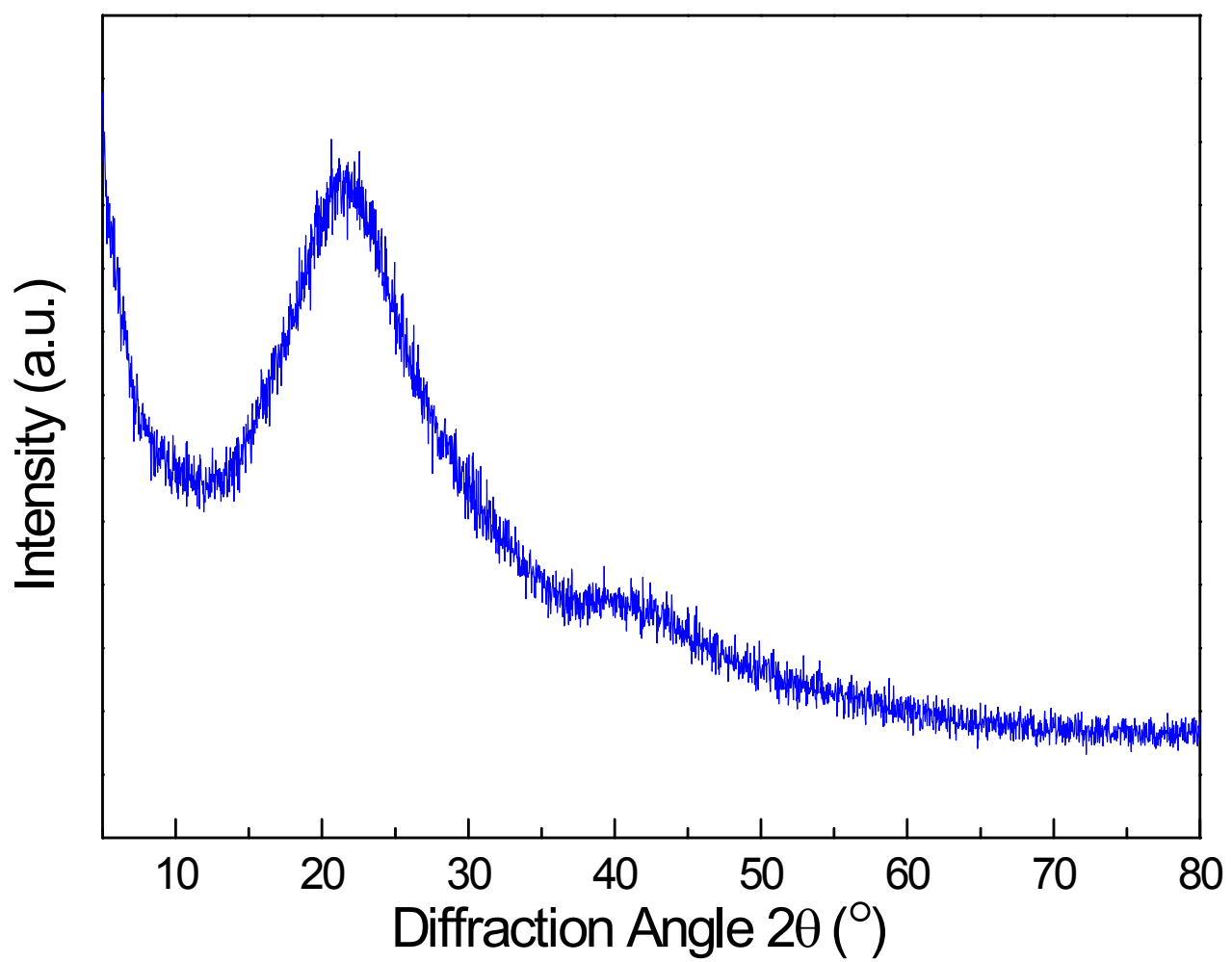


Fig. S6. XRD pattern of MNENP.

Table for comparison of specific surface area

Table-S2: Comparison of the specific surface area of various polytriazine and triazine based high surface area materials.

Organocatalysts	Synthesis method	Specific surface area (SA_{BET}) m² g⁻¹	References
P6	Cyclotrimerization	1152	S4
TFPT-COF	Cyclotrimerization	1603	S5
APOP	Schiff base condensation	724 to 1402	S6
NRPPs	Schiff base condensation	1579	S7
PCTPs	Friedal-Craft reaction	523 to 1200	S8
TSP-2	Friedal-Craft reaction	913	S9
PAF-54	Nucleophilic substitution	93	S10
NWNU-COF-1	Nucleophilic condensation	301	S11
COP-1 and COP-2	Nucleophilic condensation	168 and 158	S12
PA-1 and PA-2	Nucleophilic substitution	84.5 and 22	S13
NENPs	Nucleophilic substitution	850	S2
MNENP	Nucleophilic substitution	304	Present work

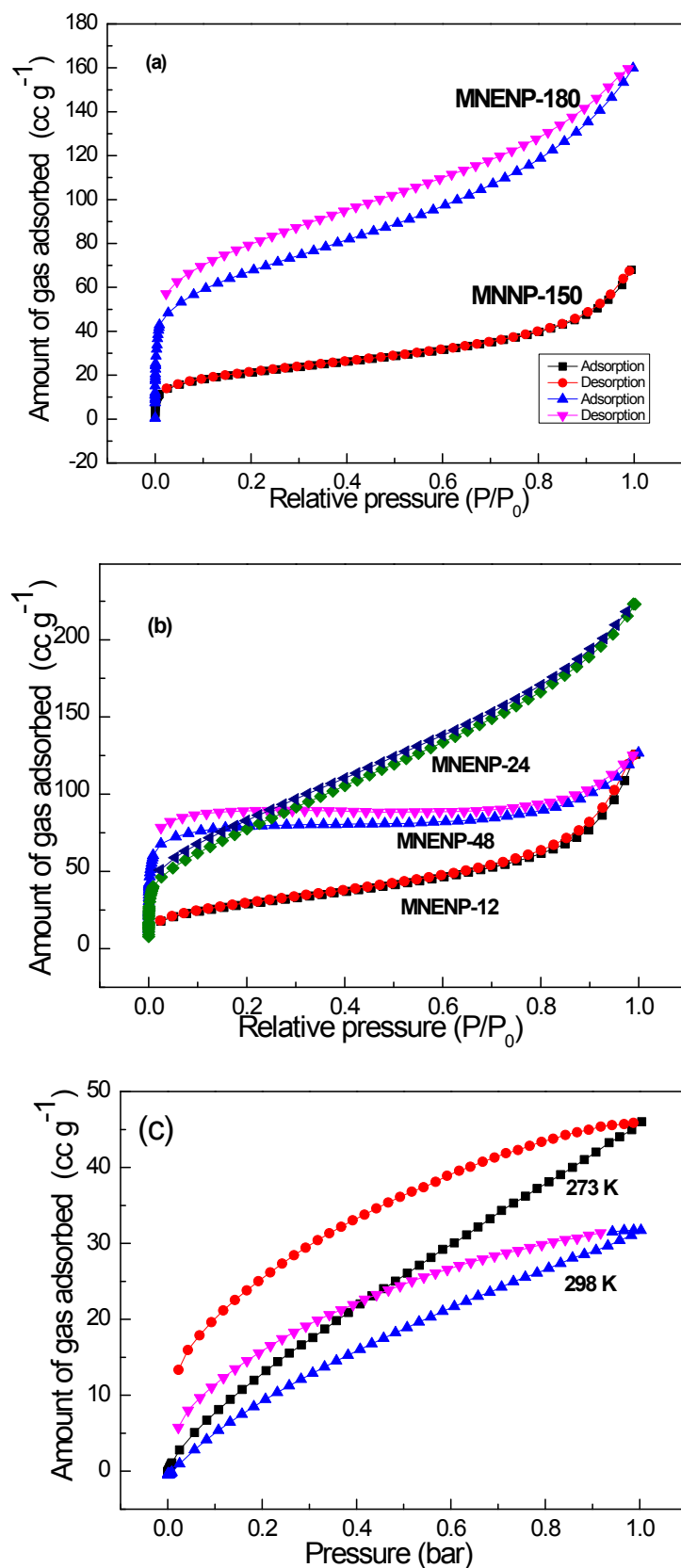


Fig. S7. Nitrogen sorption isotherm of (a) MNENP-150 and MNENP-180. (b) MNENP-12, MNENP-24, MNENP-48 and (c) CO₂ sorption isotherm at 273 and 298 K at 1 bar of MNENP.

For the confirmation of presence of different basic sites and their distribution in the framework, CO₂-TPD analysis has been performed. In general, the basic site distribution temperature ranges between 20-100 °C (weak basic sites), 300-450 °C (medium basic sites) and 500-650 °C (strong basic sites).¹⁴ The TPD profile of the MNENP (Fig. S8) has clearly depicted three CO₂ desorption peaks at about 100, 400 and 530 °C. This strongly supports the presence of weak basic sites due to –OH, medium basic sites due to –NH and strong basic sites due to aromatic nitrogen of the triazine ring present in the MNENP framework.¹⁴ The total basic sites calculated from the area under the peak from CO₂-TPD is about 2.91 mmol g⁻¹. The value is proportional to the amount of the adsorbed CO₂. The –OH groups present in the framework do not contribute in the activation of CO₂ as the experimental temperature of 100 °C is above first CO₂ desorption temperature. The medium basic sites (-NH) which are present more in the MNENP compared to that of strong basic sites largely contribute for the adsorption and activation of CO₂ during the cycloaddition reaction in the absence of co-catalyst for the synthesis of cyclic carbonates.

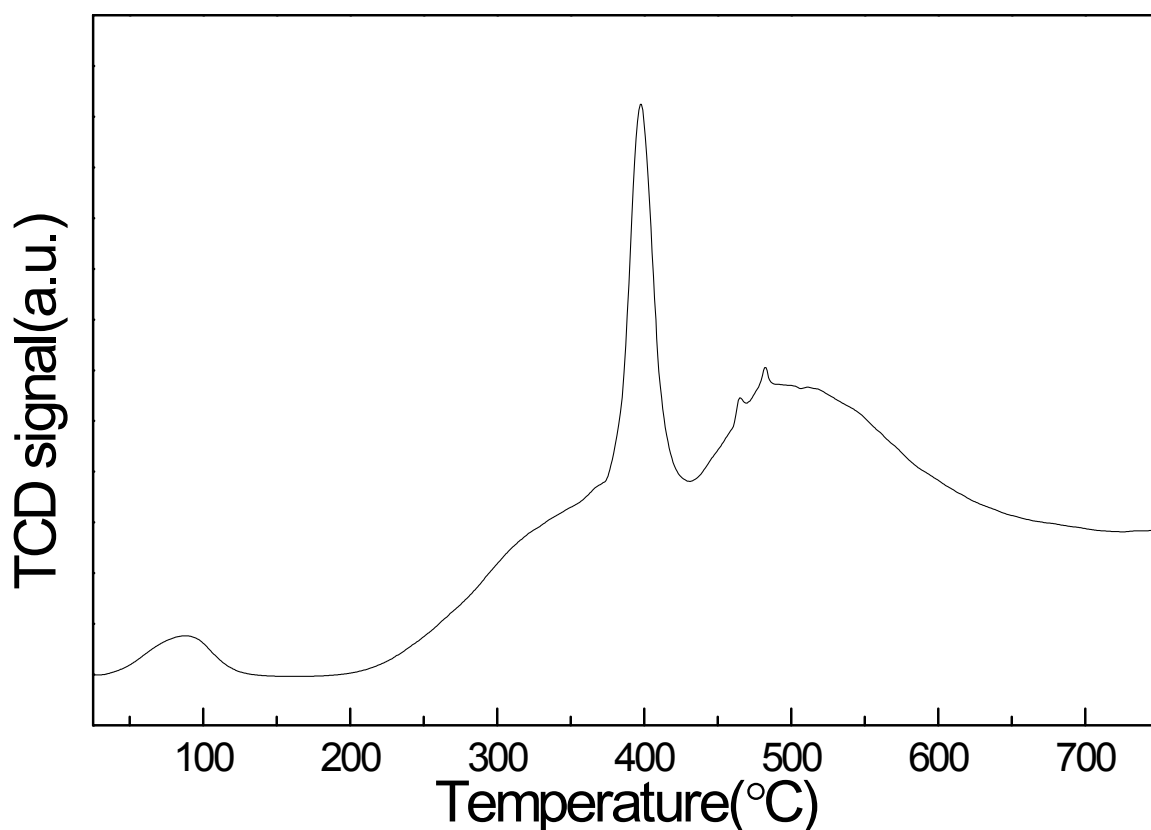


Fig. S8. CO₂-TPD profile of MNENP.

4. Characterization of cyclic carbonates

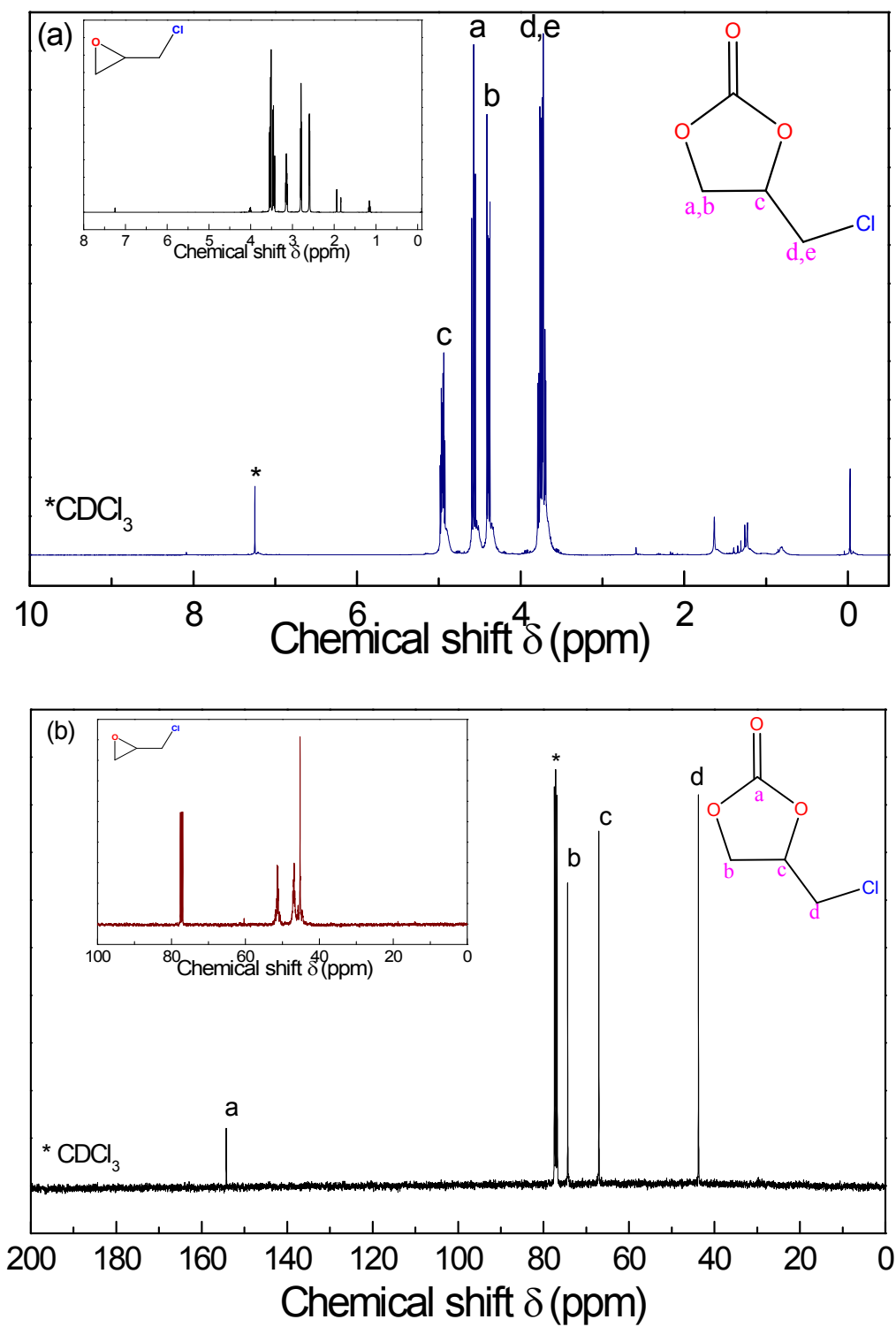


Fig. S9. (a) ^1H and (b) ^{13}C NMR spectra of 4-(Chloromethyl)-1,3-dioxolan-2-one.

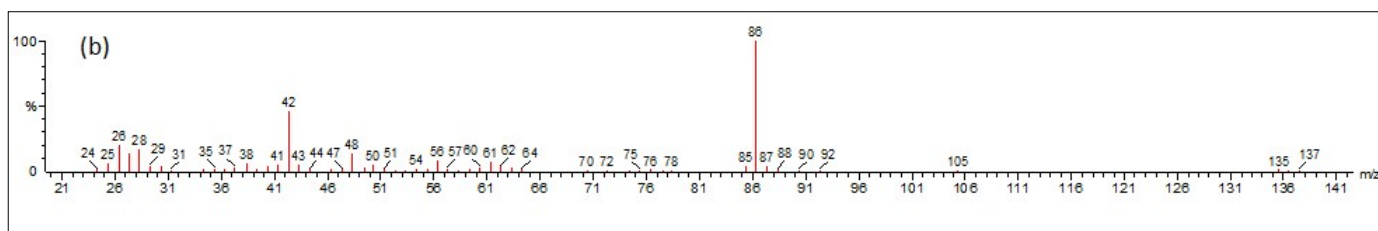
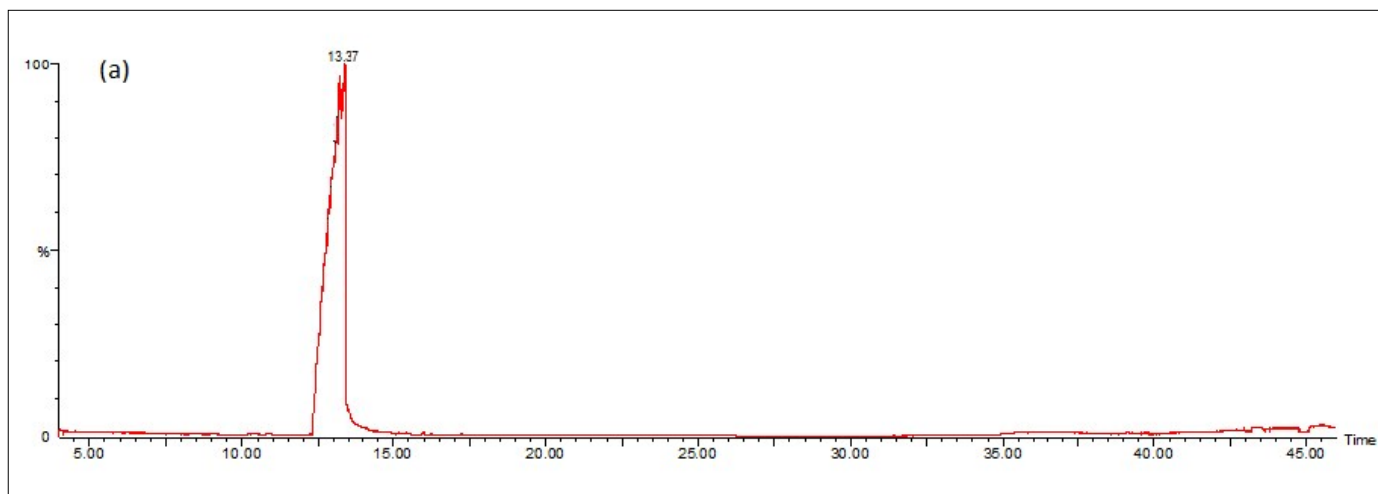


Fig. S10. (a) GC and (b) MS spectrum of 4-(Chloromethyl)-1,3-dioxolan-2-one.

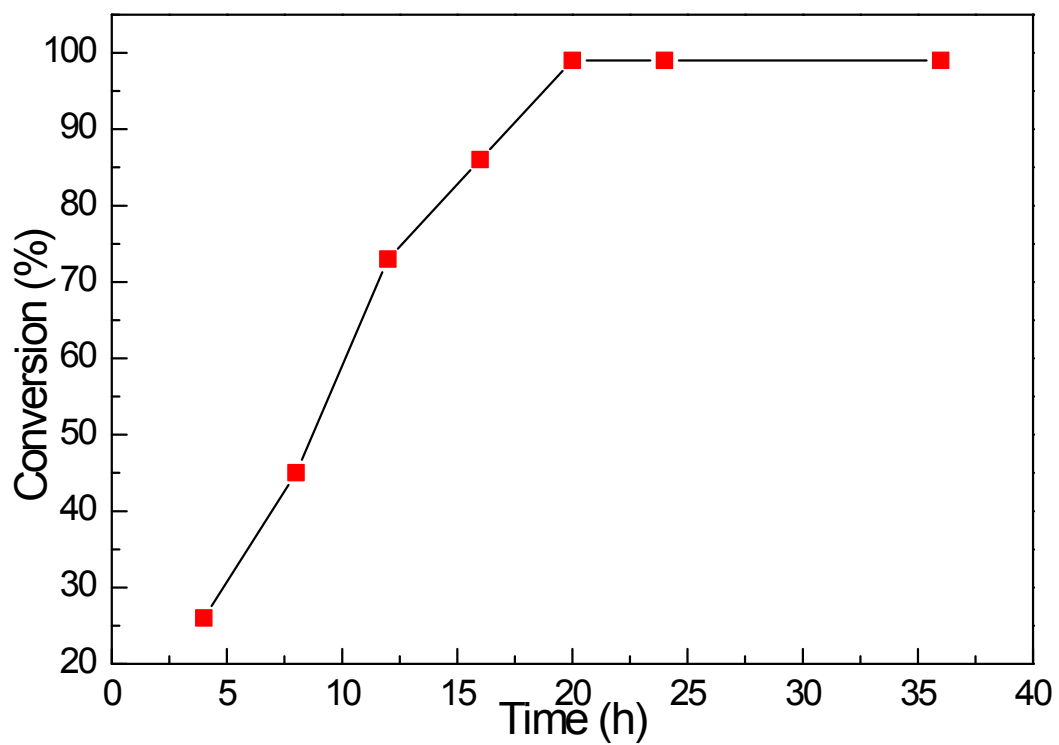


Fig. S11. Kinetics studies of cycloaddition of epoxide and CO₂ at 100 °C using 0.25 ml of epichlorohydrin as model substrate, 10 mg catalyst at different time.

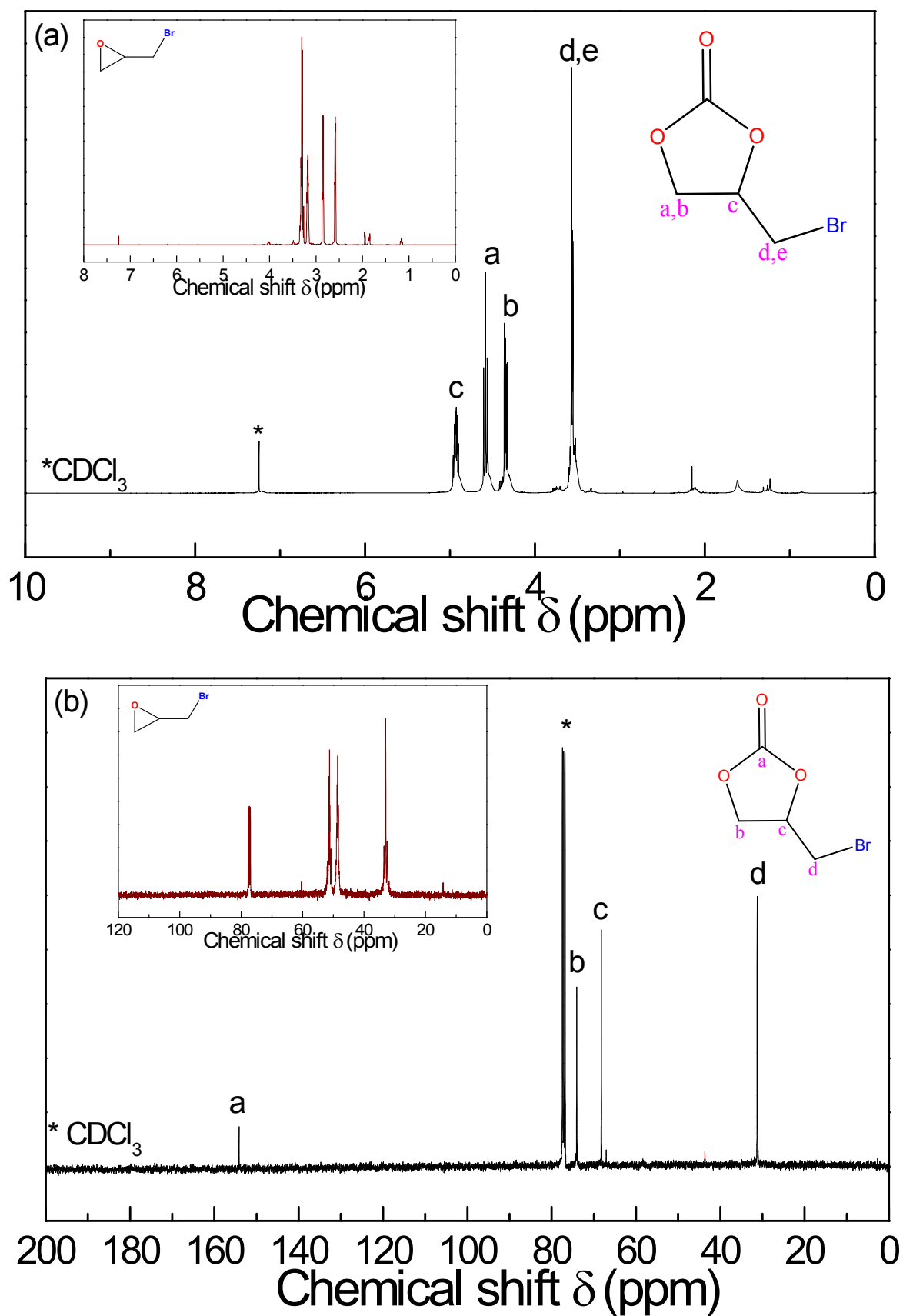


Fig. S12. (a) ¹H and (b) ¹³C NMR spectra of 4-(Bromomethyl)-1,3-dioxolan-2-one.

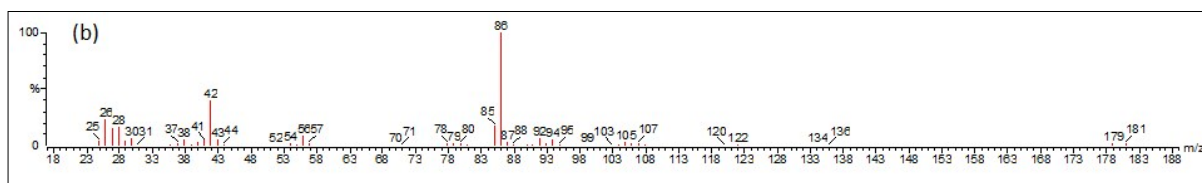
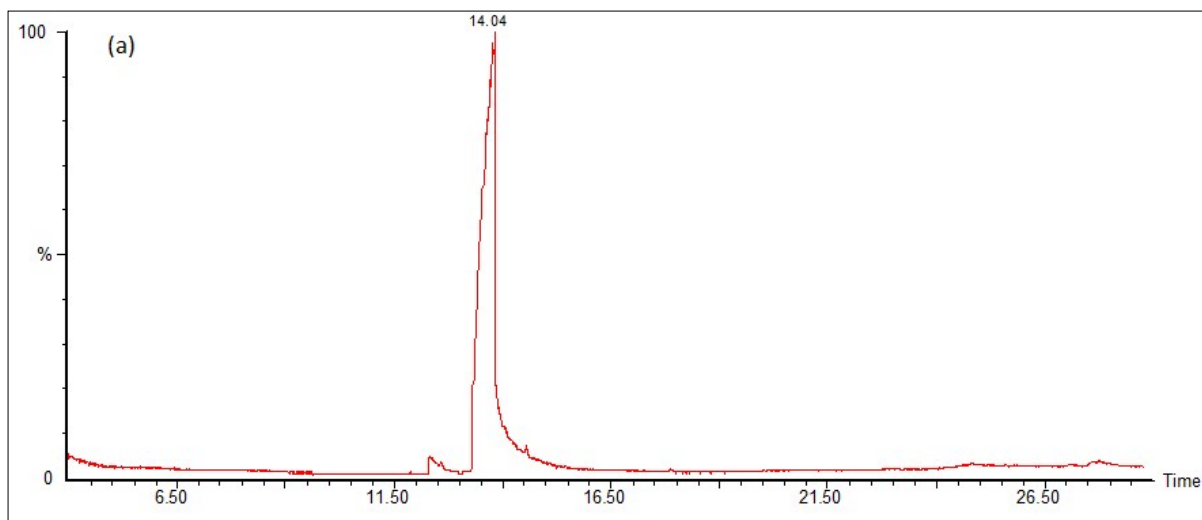


Fig. S13. (a) GC and (b) MS spectrum of 4-(Bromomethyl)-1,3-dioxolan-2-one.

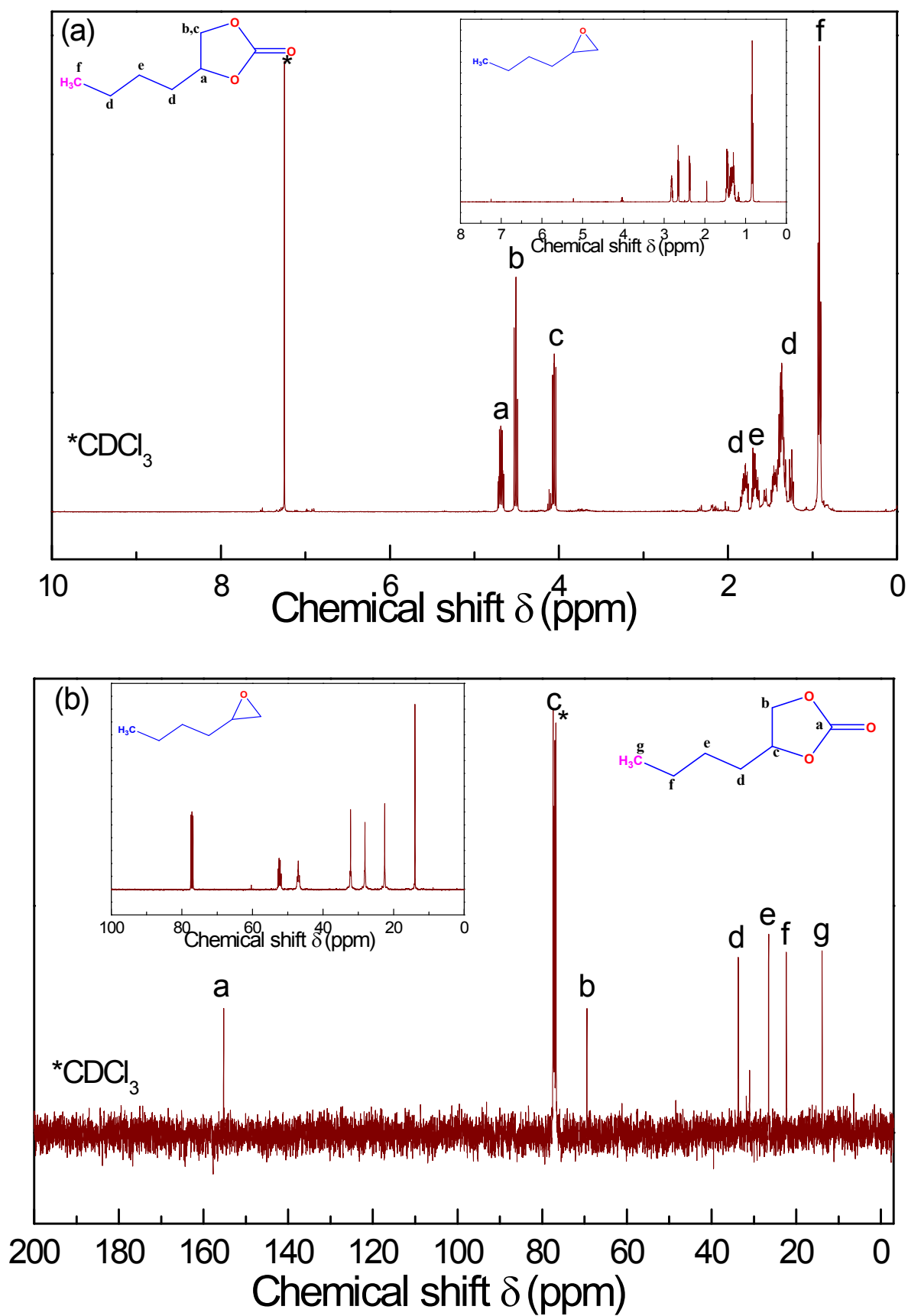


Fig. S14. (a) ^1H and (b) ^{13}C NMR spectra of 4-Butyl-1,3-dioxolan-2-one.

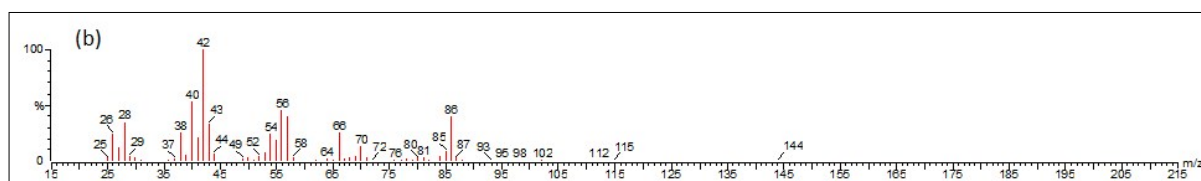
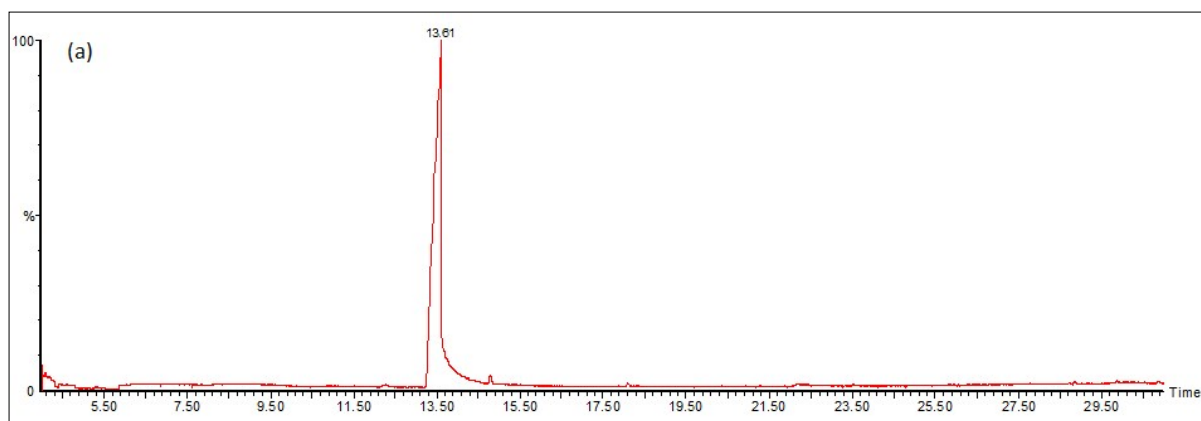


Fig. S15. (a) GC and (b) MS spectrum of 4-Butyl-1,3-dioxolan-2-one.

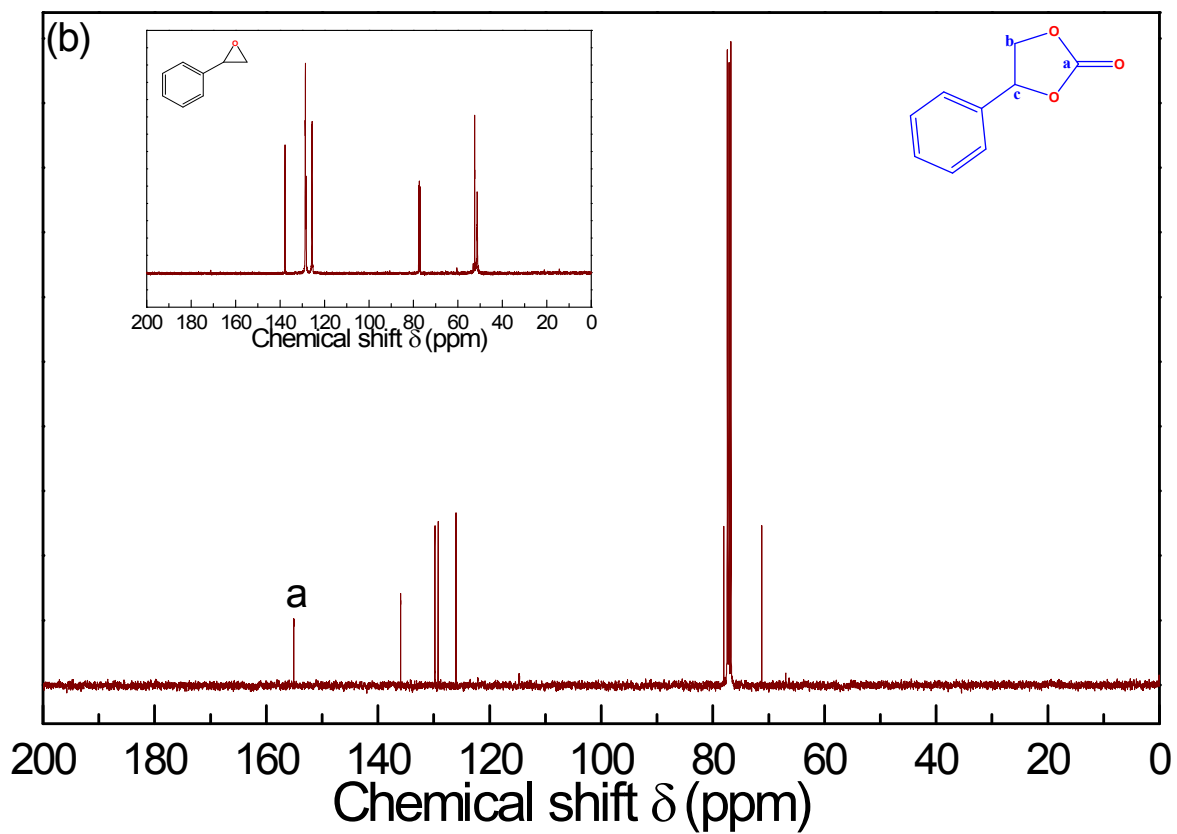
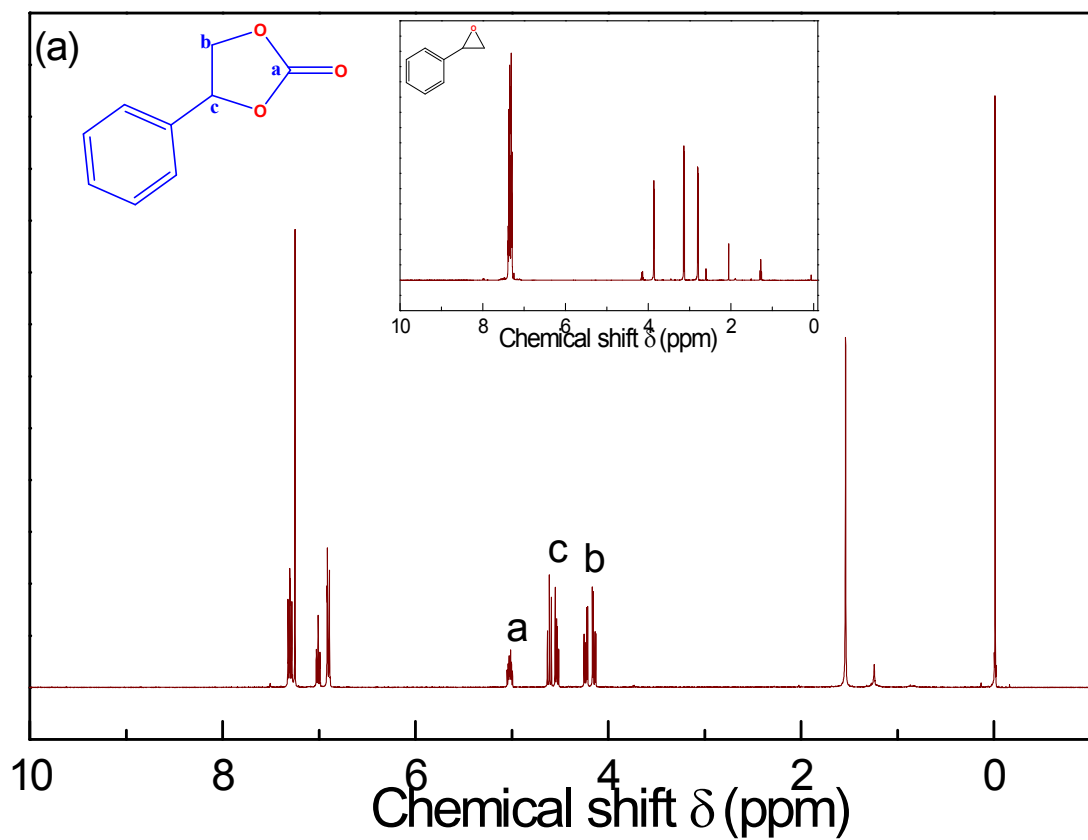


Fig. S16. (a) ^1H and (b) ^{13}C NMR spectra of 4-Phenyl-1,3-dioxolan-2-one.

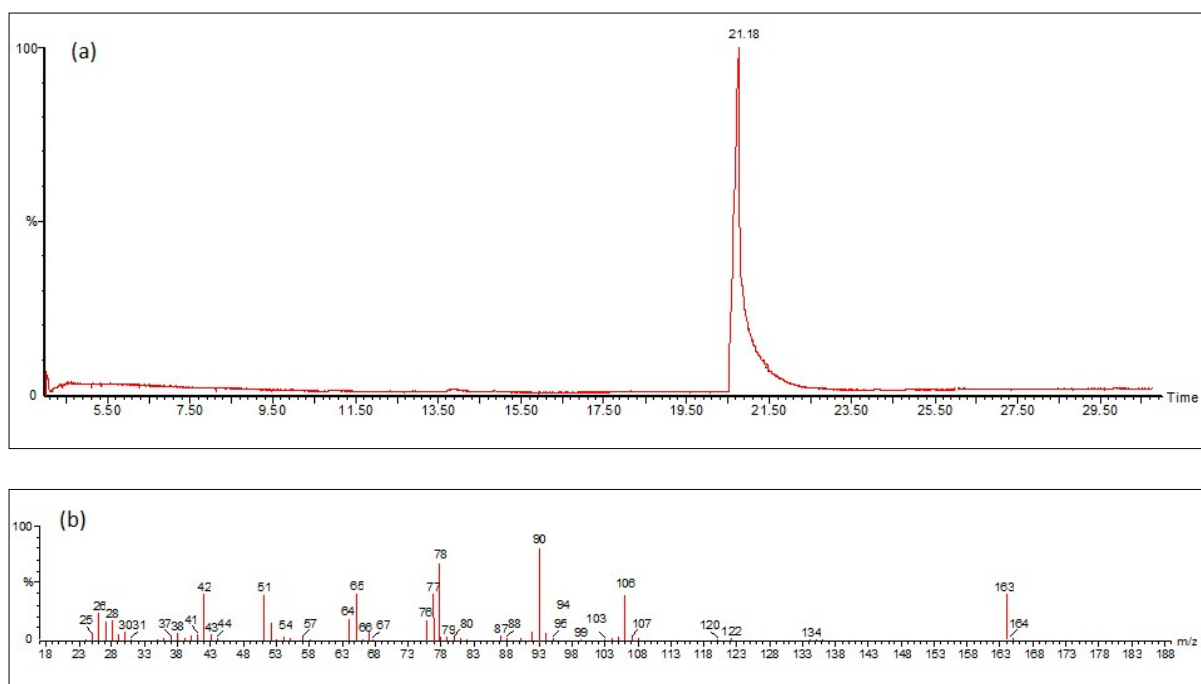


Fig. S17. (a) GC and (b) MS spectrum of 4-Phenyl-1,3-dioxolan-2-one.

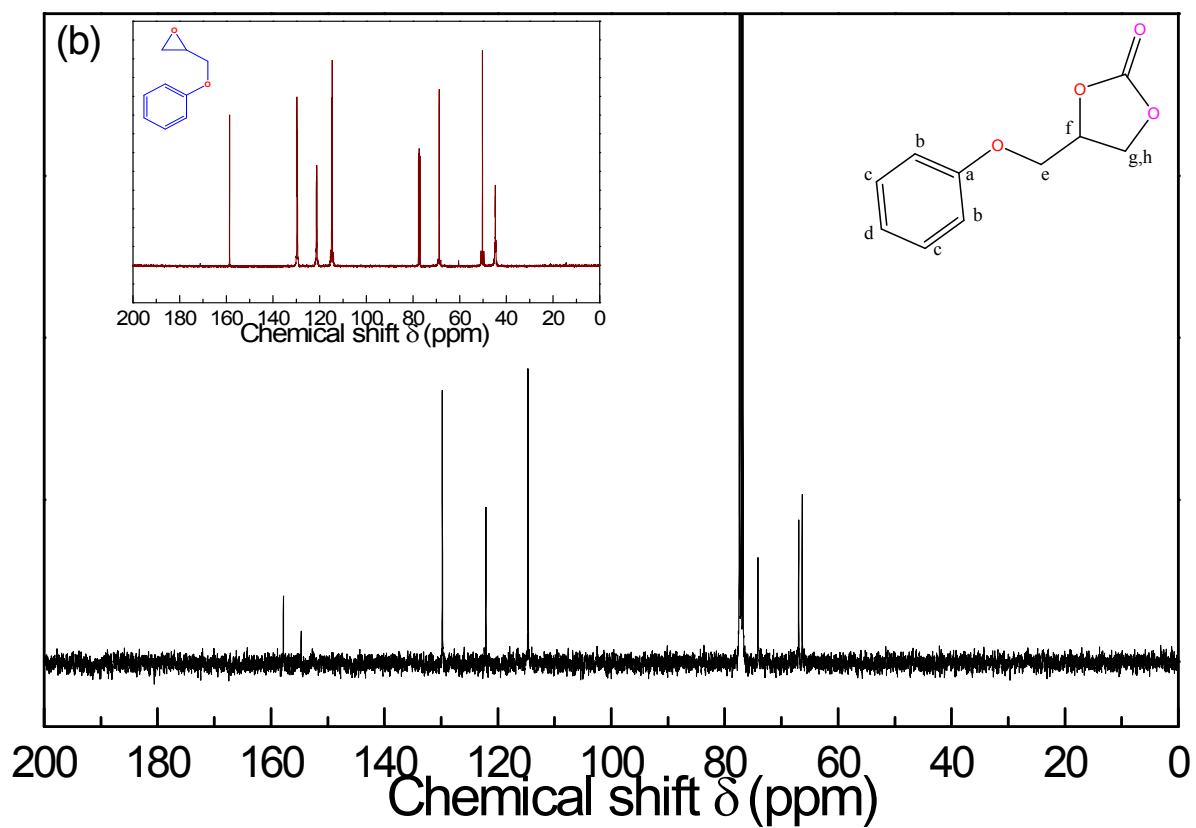
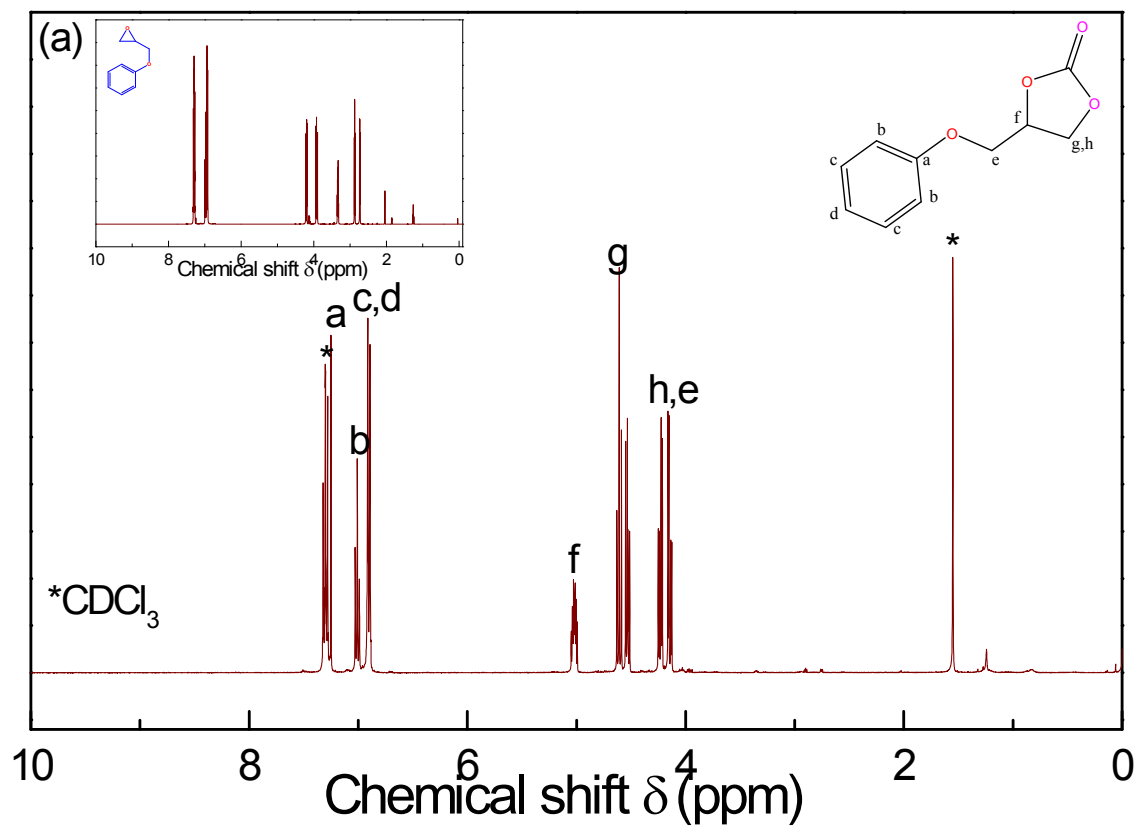


Fig. S18. (a) ¹H and (b) ¹³C NMR spectra of 4-(Phenoxy methyl)-1,3-dioxolan-2-one.

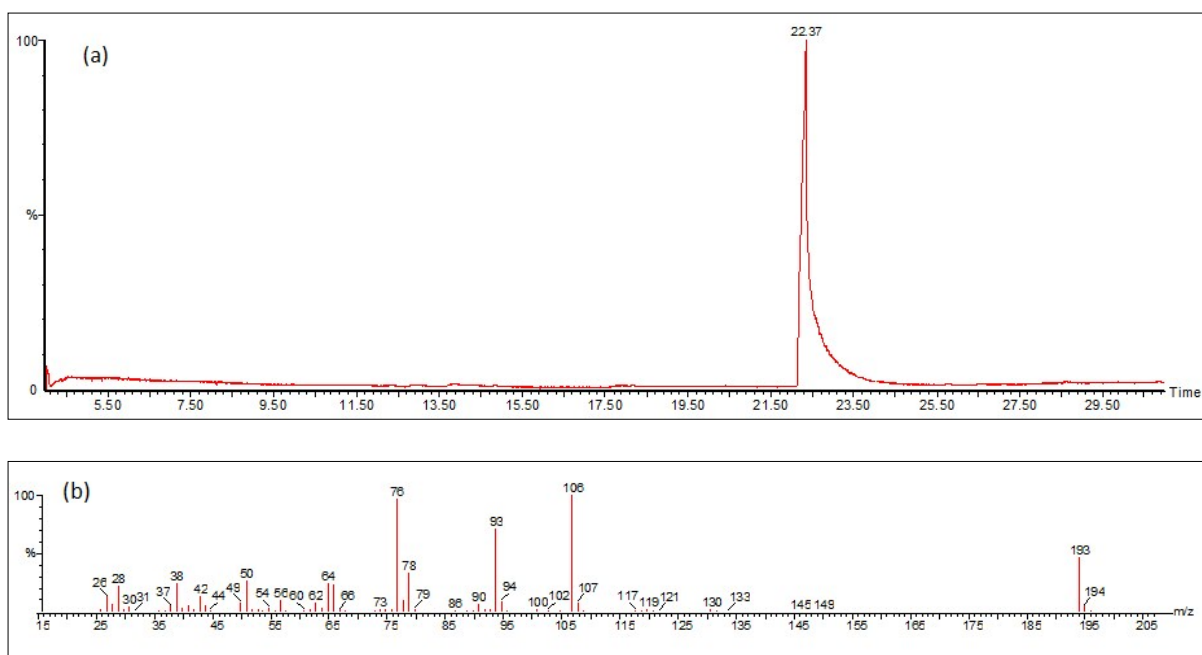


Fig. S19. (a) GC and (b) MS spectrum of 4-(Phenoxy methyl)-1,3-dioxolan-2-one.

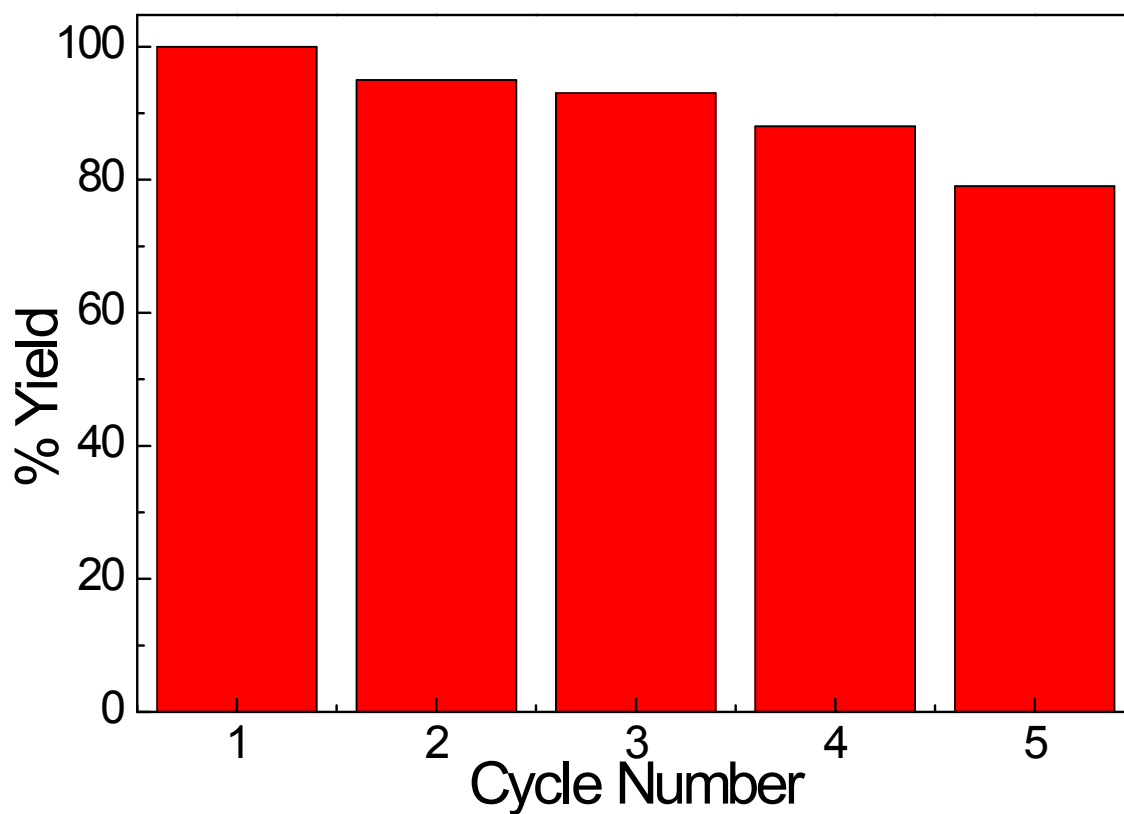


Fig. S20. Catalytic recycling study of MNENP catalyzed CO₂ conversion.

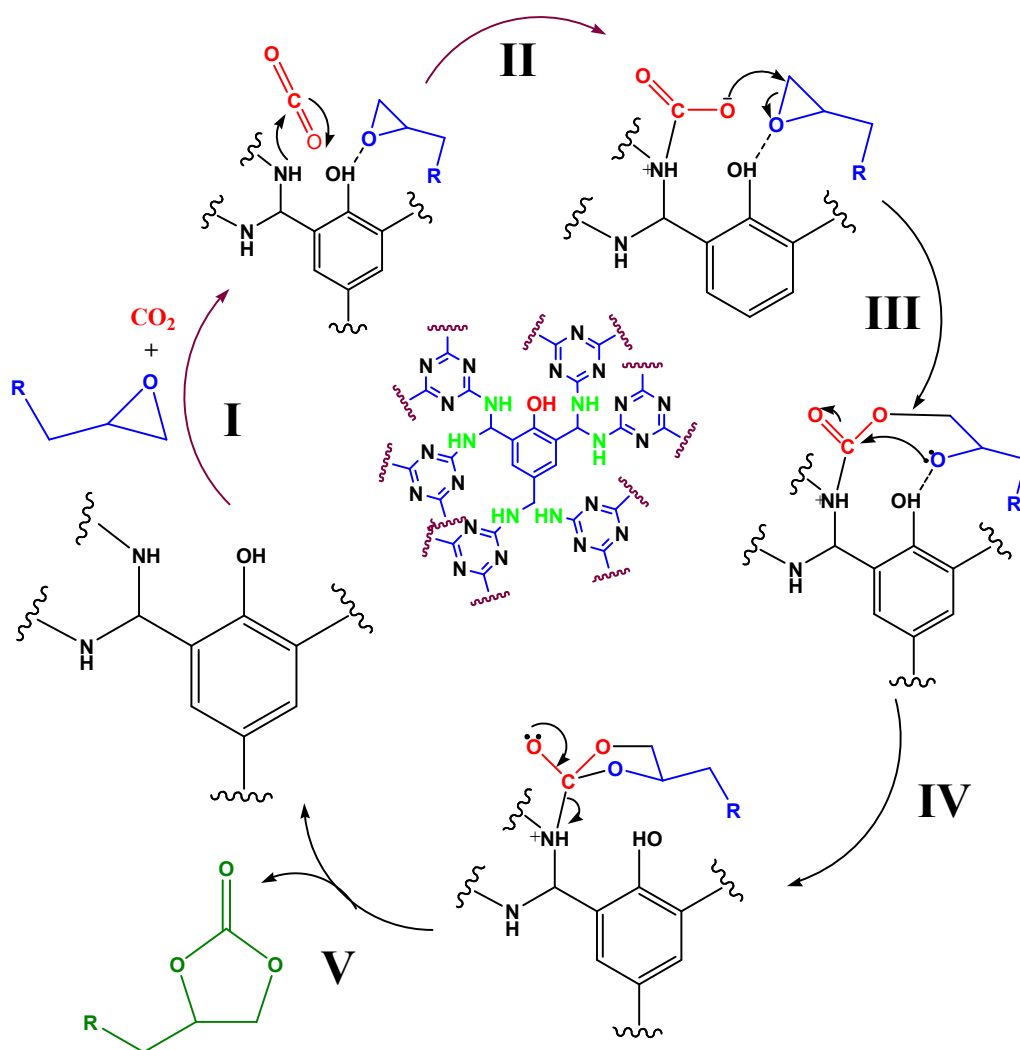


Fig. 21. Plausible mechanism of MNENP catalysed synthesis of cyclic carbonates via cycloaddition of epoxides and CO₂.

5. Theoretical calculations

To get more insight on the role of -OH group in the interaction between the MNENP moiety and epoxide molecules, density functional theoretical calculations were also carried out.¹⁵ For this purpose, we optimized the geometries of the complexes formed between the epoxide molecule and the framework, the latter with and without hydroxyl group. The hybrid density functional B3LYP in conjunction with 6-311+G** basis set was used for the calculations. The optimized geometries of the above complexes are depicted in Fig. S21. The studies revealed that the interaction energy of epoxide with the hydroxylated framework (MNENP) is ~ 4 kcal/mol more than that for the framework without the hydroxyl group. This is understandable due the stronger hydrogen bond interaction between the oxygen atom of epoxide with -OH group of the framework that activate the reaction for the formation of the desired product.

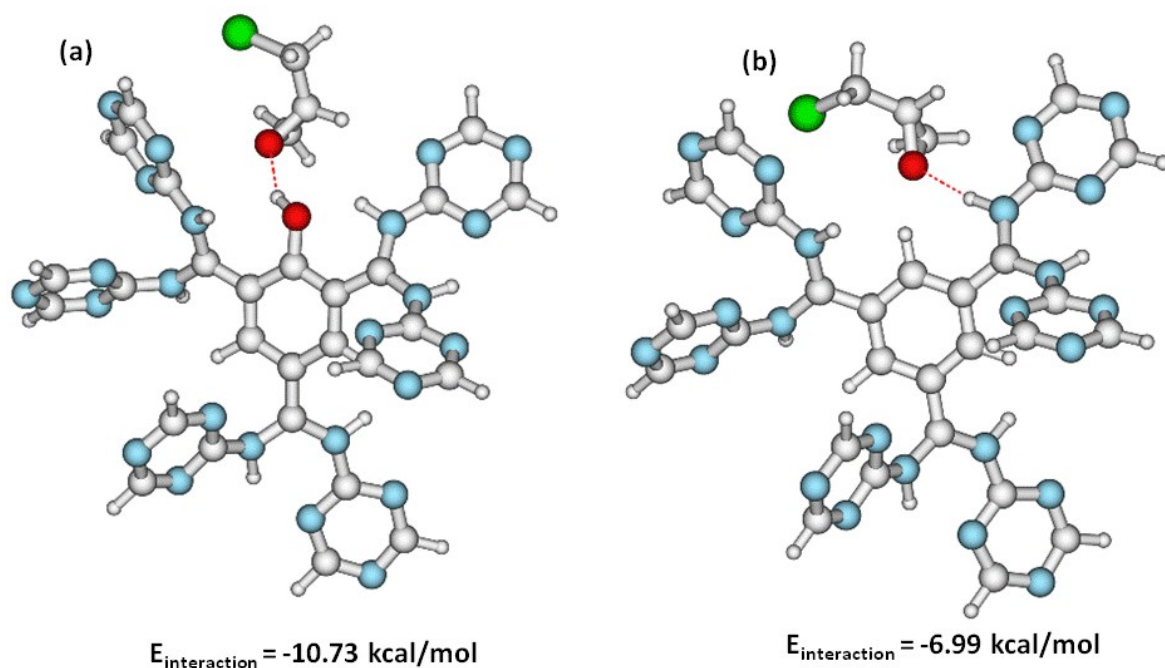


Fig. S22. The optimized geometries of the complex formed between epoxide and the framework (a) with and (b) without hydroxyl group obtained at B3LYP/6-311+G** level.

6. Characterization of methanol

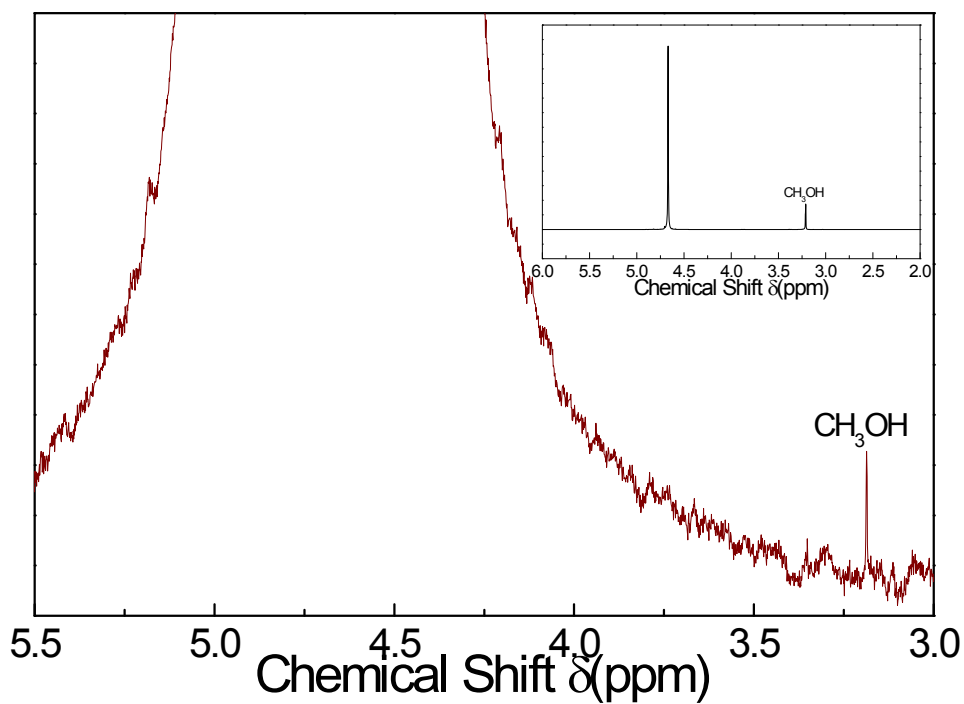


Fig. S23. ¹H NMR spectra of 0.1 M KHCO₃ electrolyte after electrocatalysis by MNENP showing the peak for CH₃OH at 3.21 ppm in D₂O solvent (inset: ¹H NMR of standard methanol in D₂O).

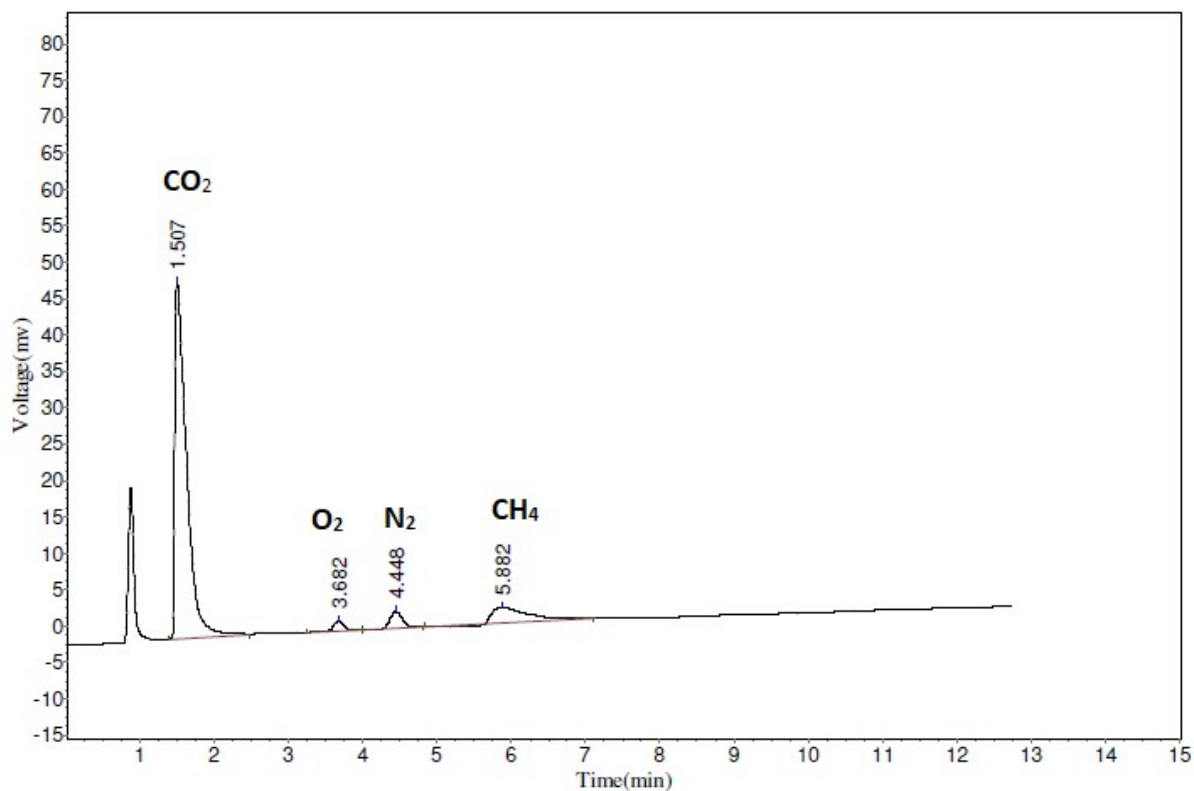


Fig. S24. GC chromatogram of the products after 4 h reduction of CO_2 on MNENP.

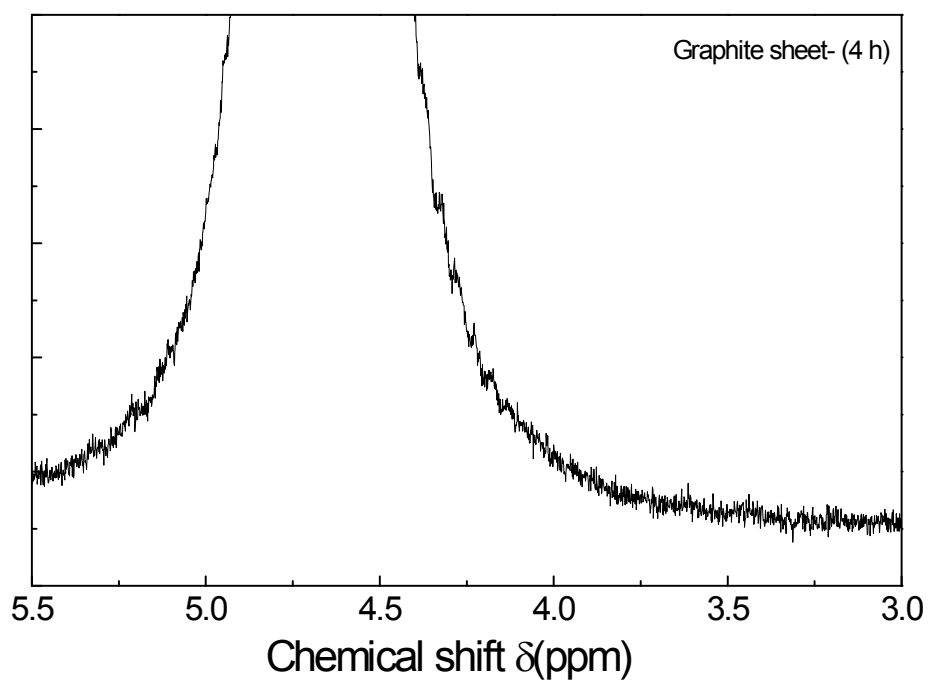
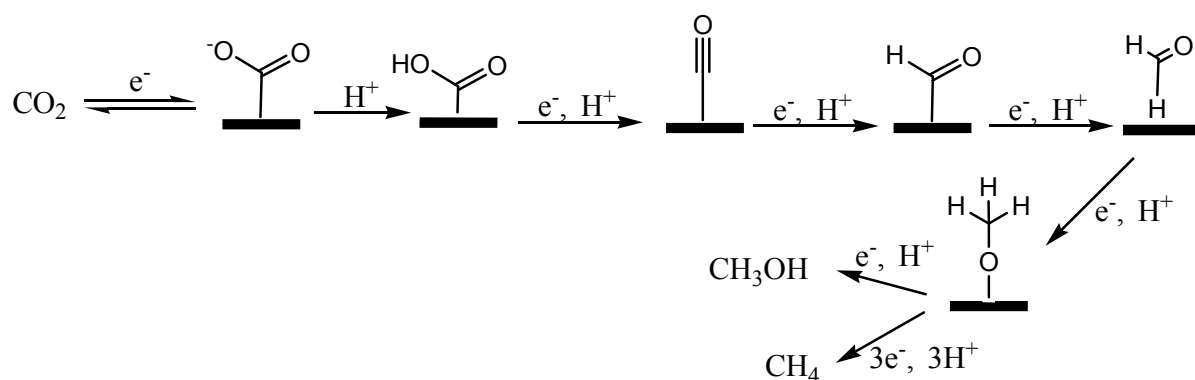


Fig. S25. ^1H NMR spectra of 0.1 M KHCO_3 electrolyte after electrocatalysis in D_2O solvent.

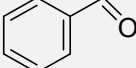
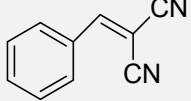
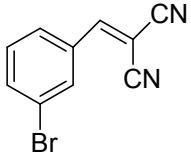
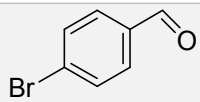
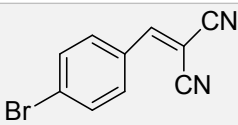
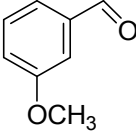
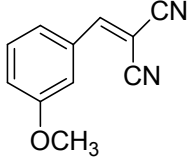
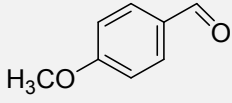
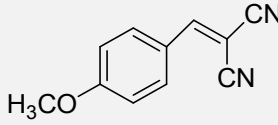
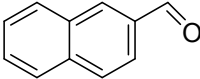
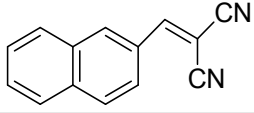
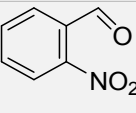
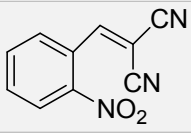
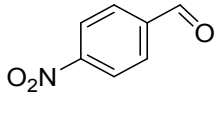
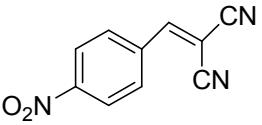
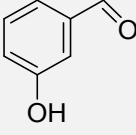
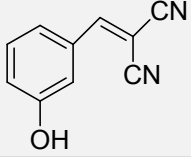
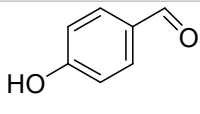
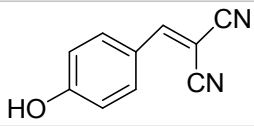
Mechanism for Electrochemical reduction of CO₂



Scheme S4: Mechanism for the formation of methanol and methane by the electroreduction of CO₂ using MNENP as electrocatalyst.

7. Table for Knoevenagel reaction

Table S3: MNENP catalyzed C-C bond formation between various aldehyde and malononitrile via Knoevenagel condensation.

S.No.	Aldehyde	Product	Yield
1.			95
2.			92
3.			90
4.			84
5.			87
6.			81
7.			80
8.			72
9.			46
10.			50

Catalyst =10 mg; aromatic aldehyde = 1 mmol; Malononitrile = 1mmol; Time = 4 h, RT.

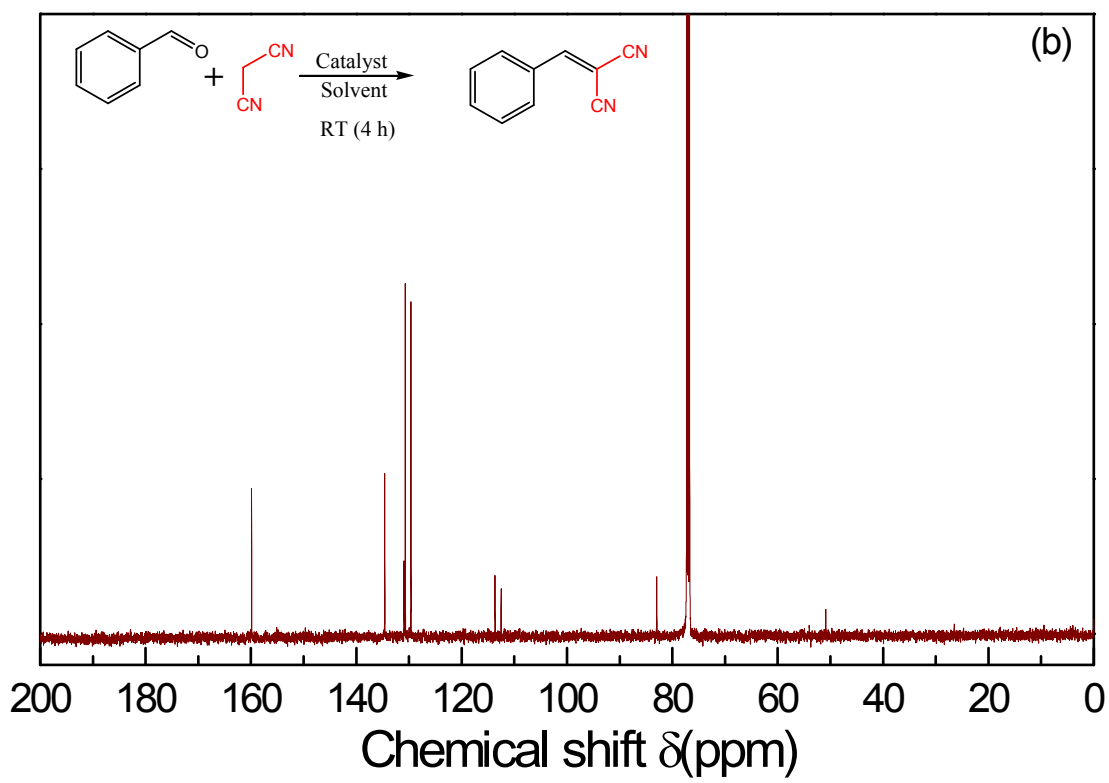
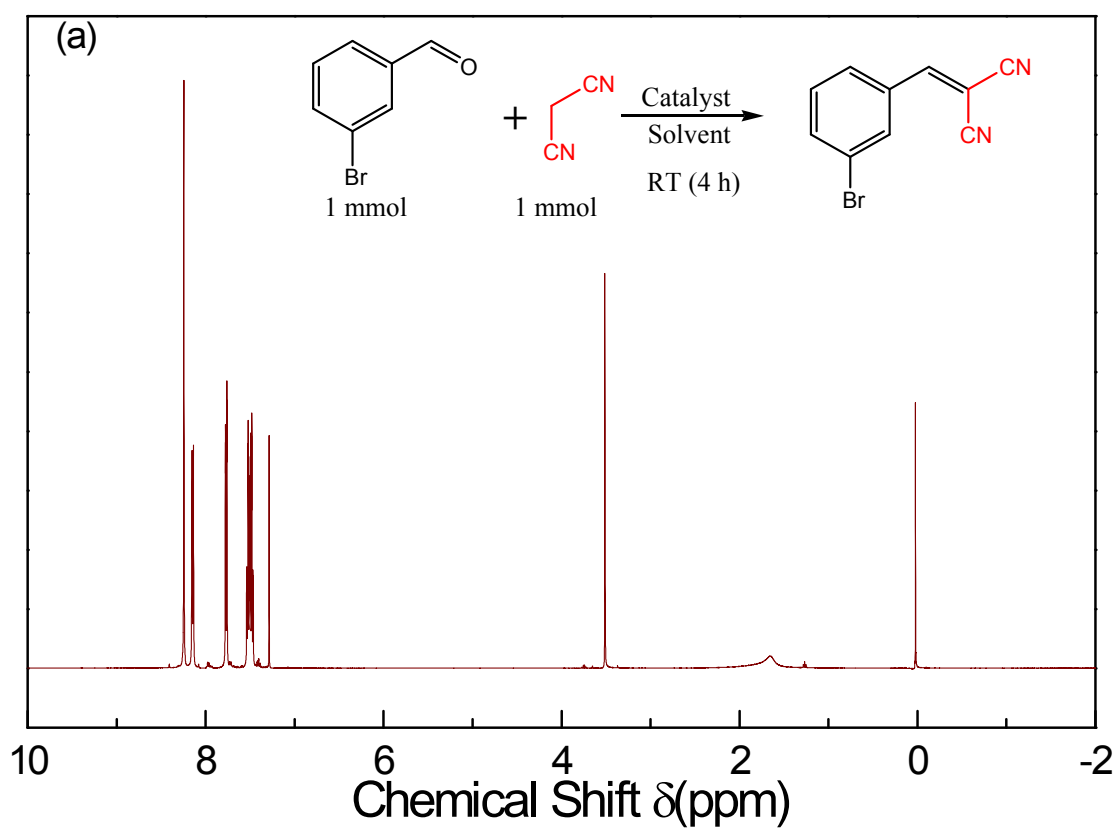


Fig. S26. (a) ^1H and (b) ^{13}C NMR spectra of benzylidene malononitrile.



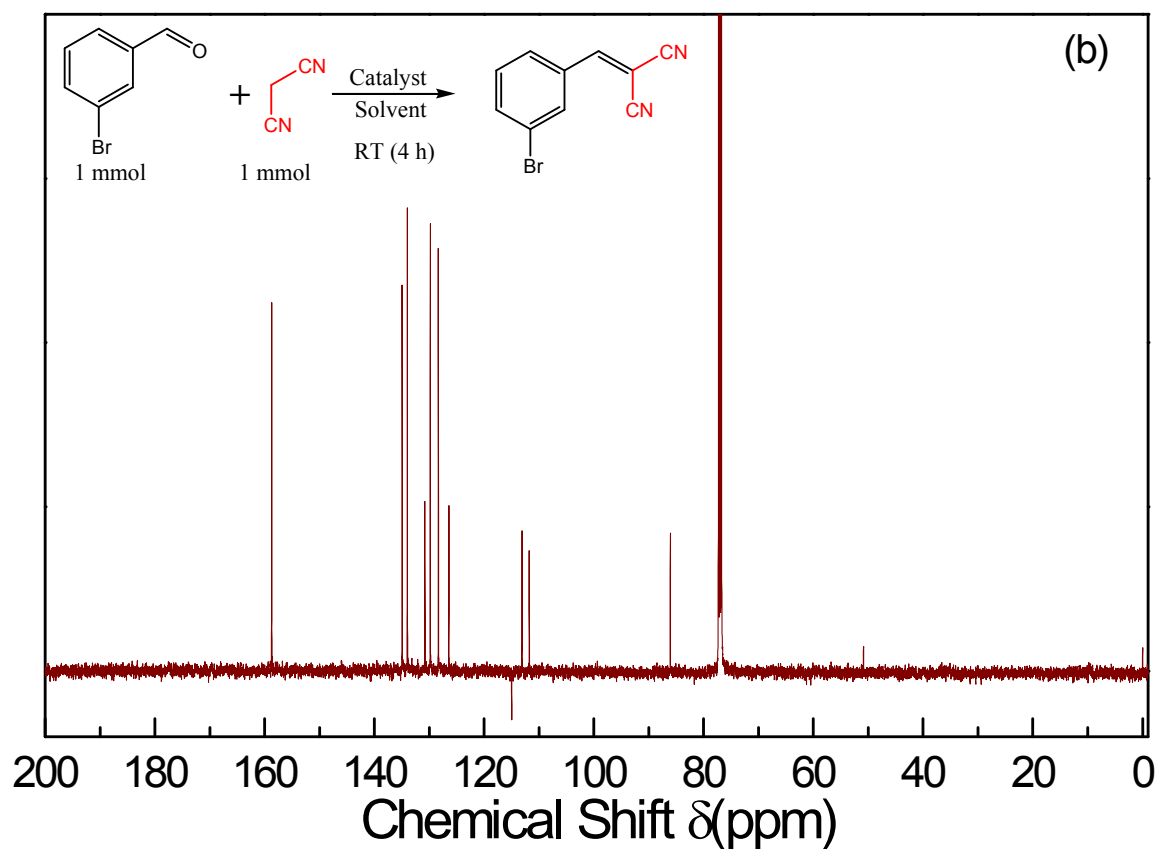
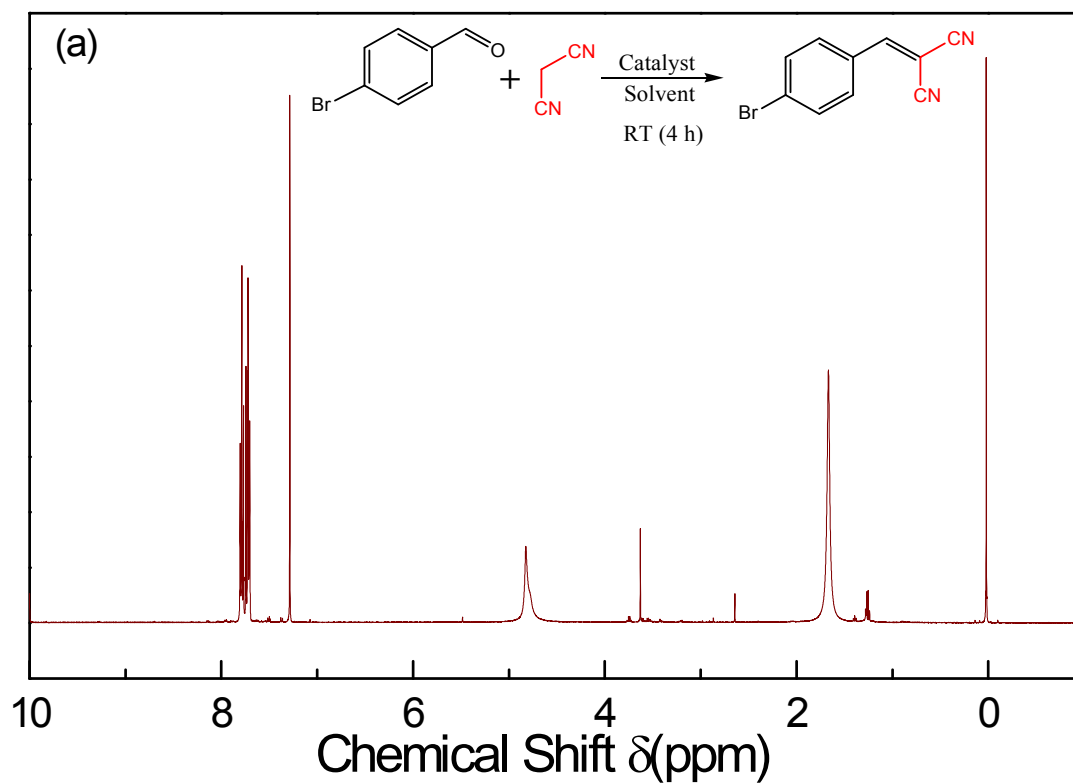


Fig. S27. (a) ^1H and (b) ^{13}C NMR spectra of 3-Bromo benzylidene malononitrile.



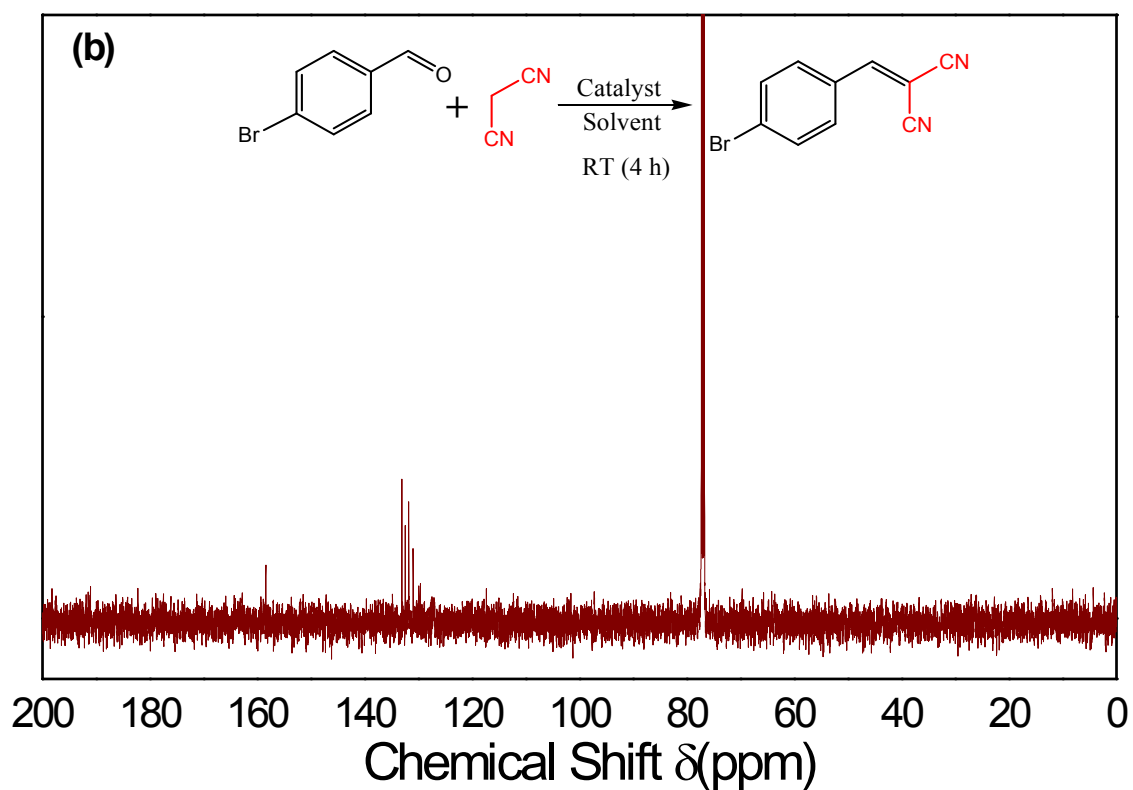
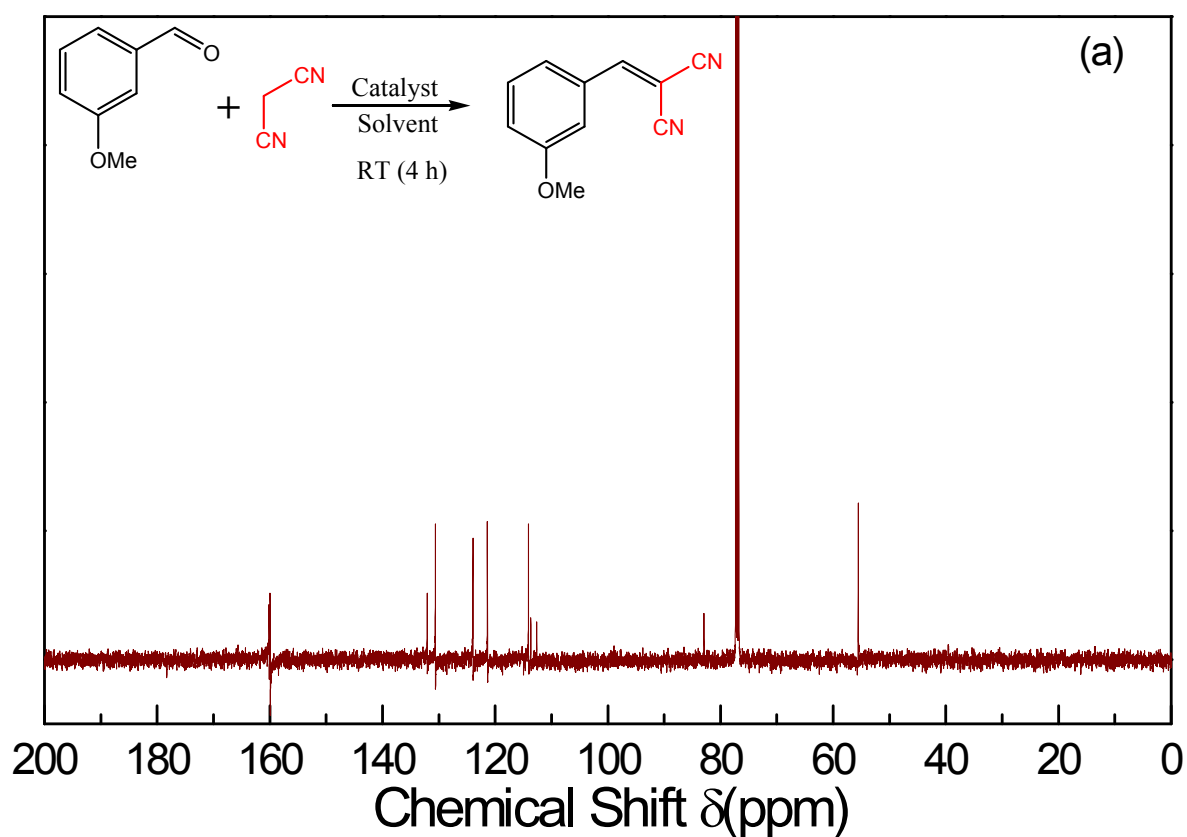


Fig. S28. (a) ^1H and (b) ^{13}C NMR spectra of 4-Bromo benzylidene malononitrile.



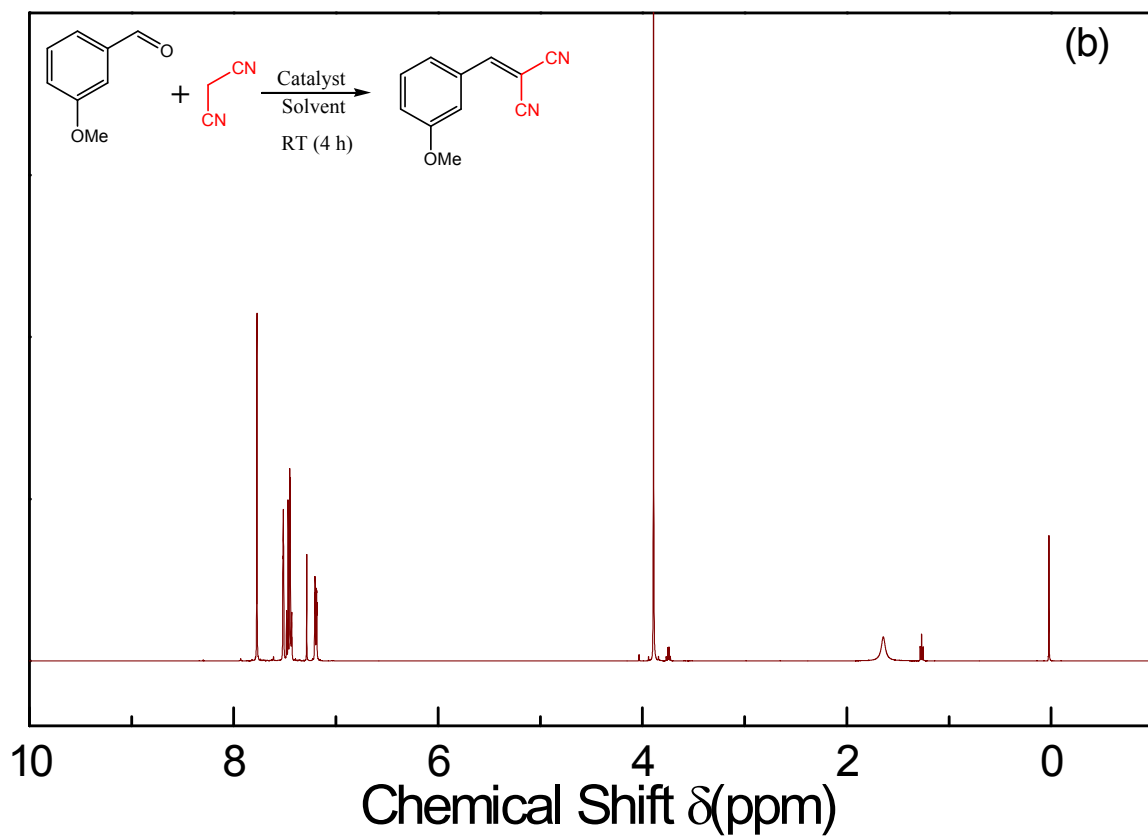
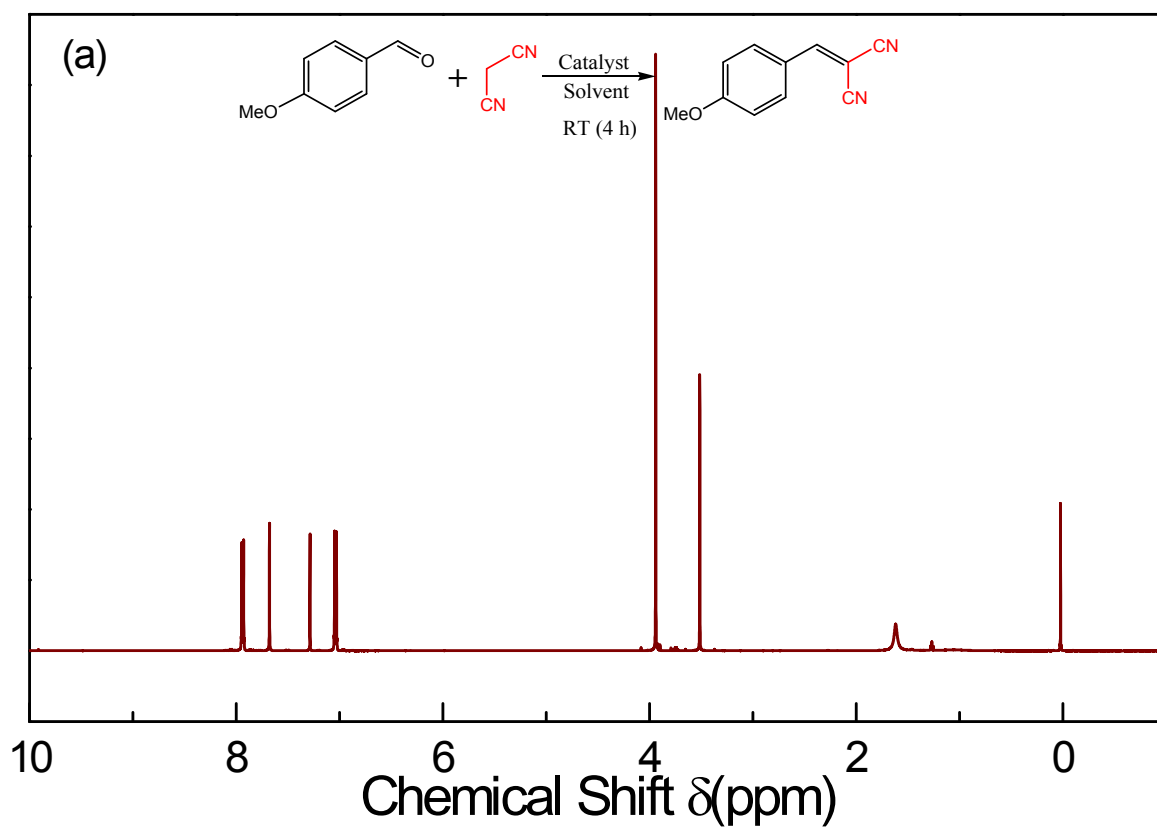


Fig.S29. (a) ^1H and (b) ^{13}C NMR spectra of 3-methoxy benzylidene malononitrile.



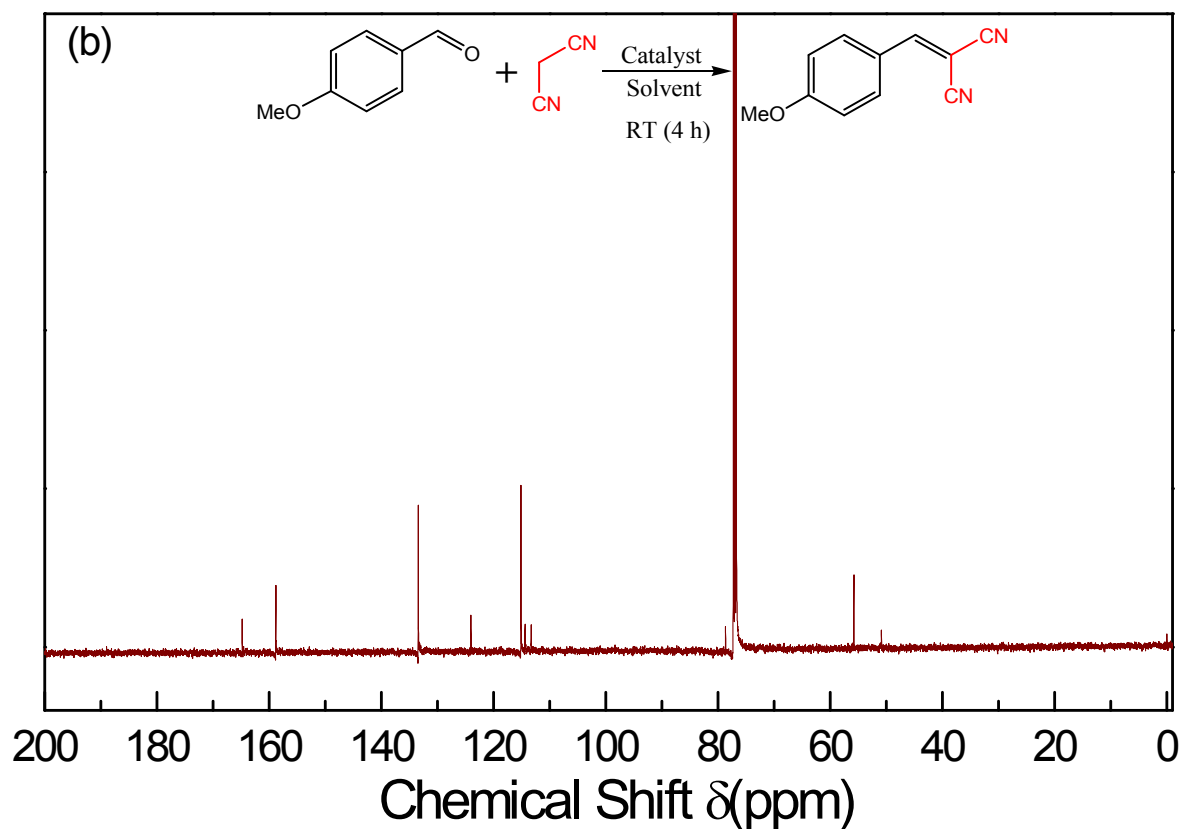
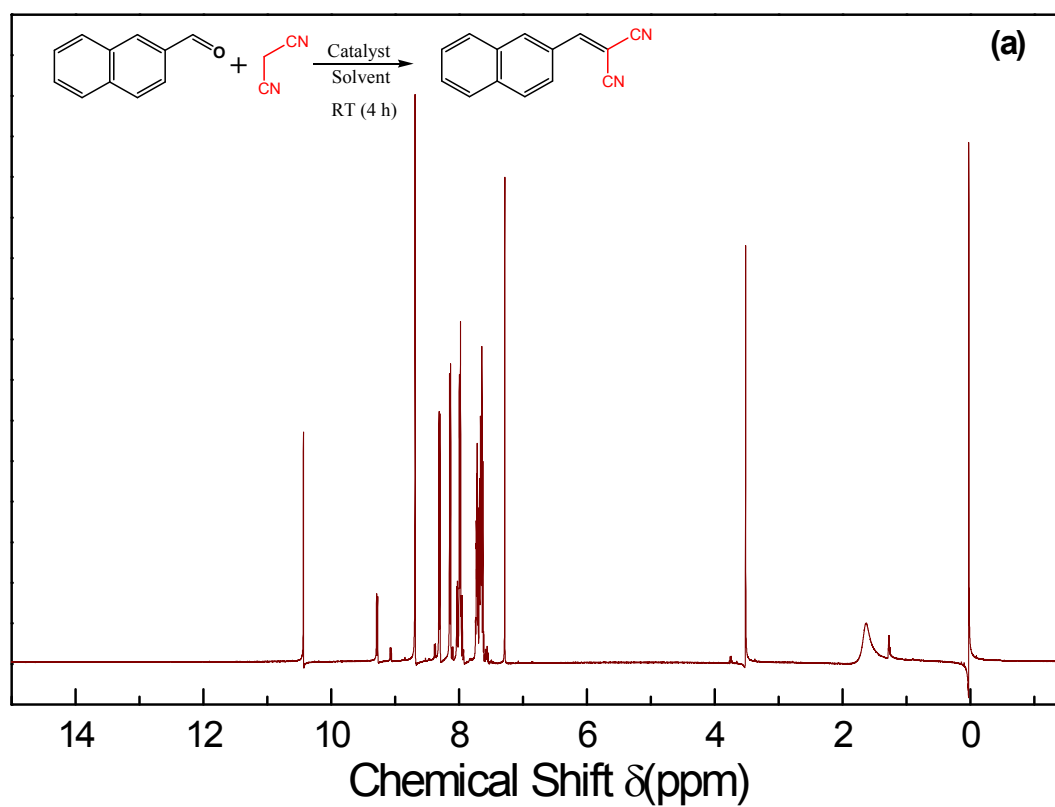


Fig. S30. (a) ^1H and (b) ^{13}C NMR spectra of 4-methoxy benzylidene malononitrile.



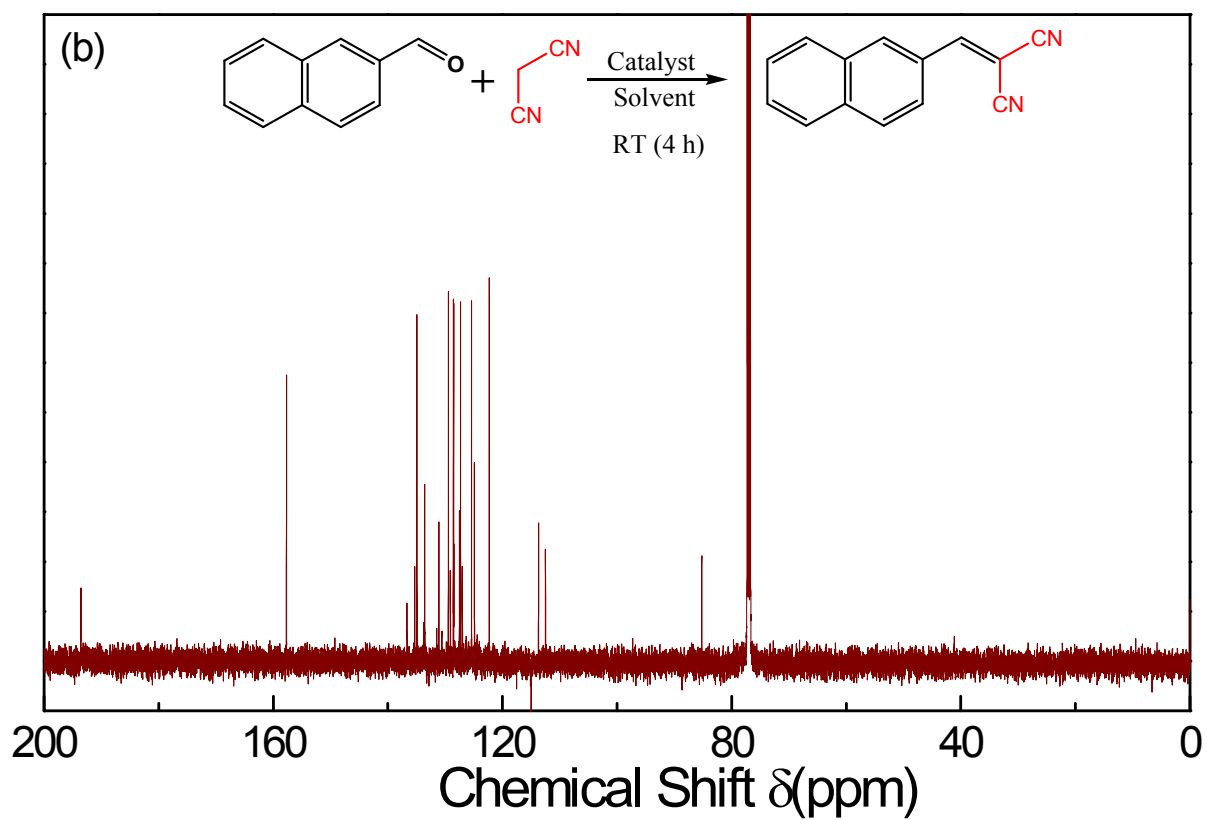


Fig. S31. (a) ^1H and (b) ^{13}C NMR spectra of 2-(2-naphthalenylmethylene)- Propanedinitrile.

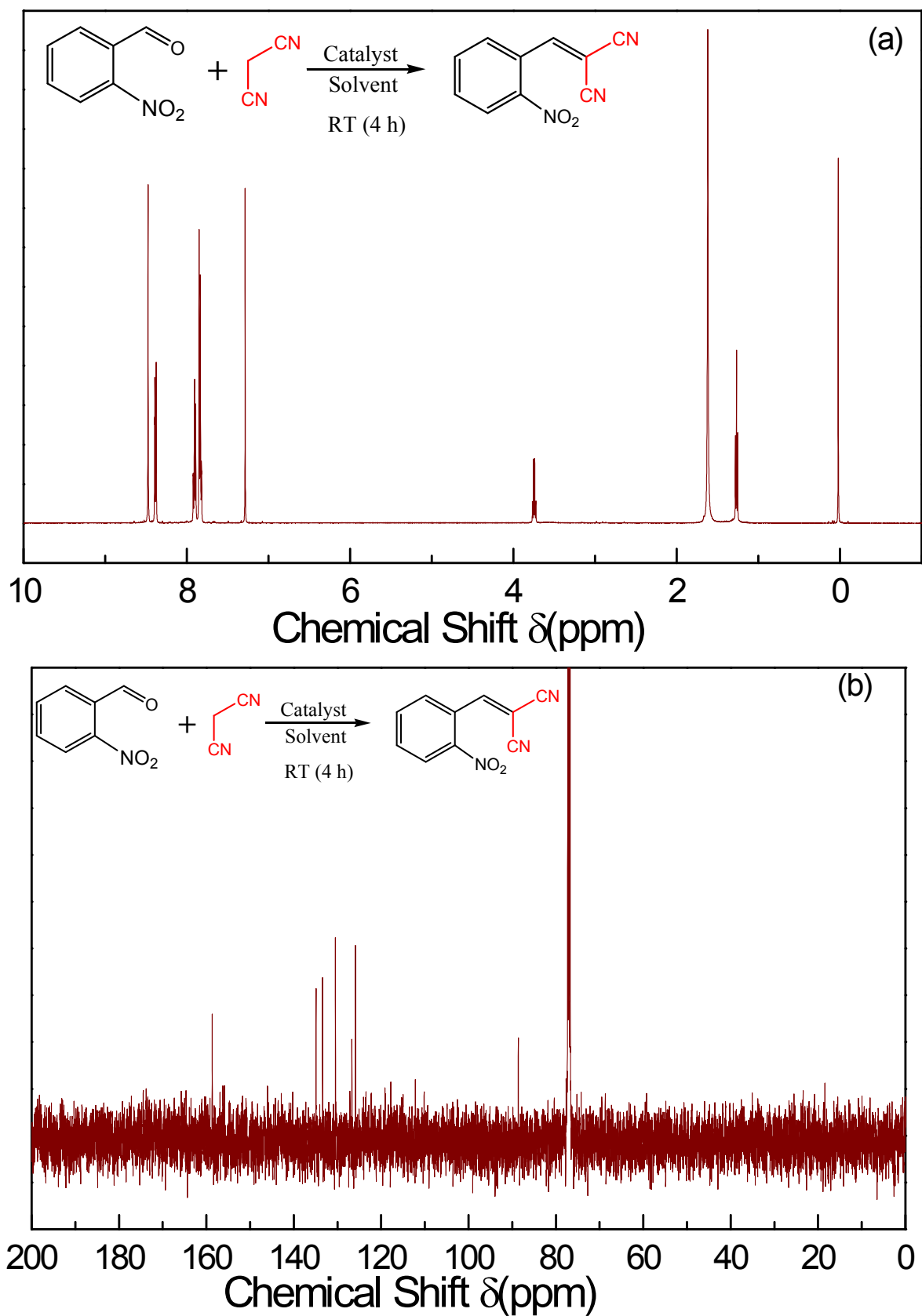


Fig. S32. (a) ^1H and (b) ^{13}C NMR spectra of 2-Nitro benzylidinemalononitrile.

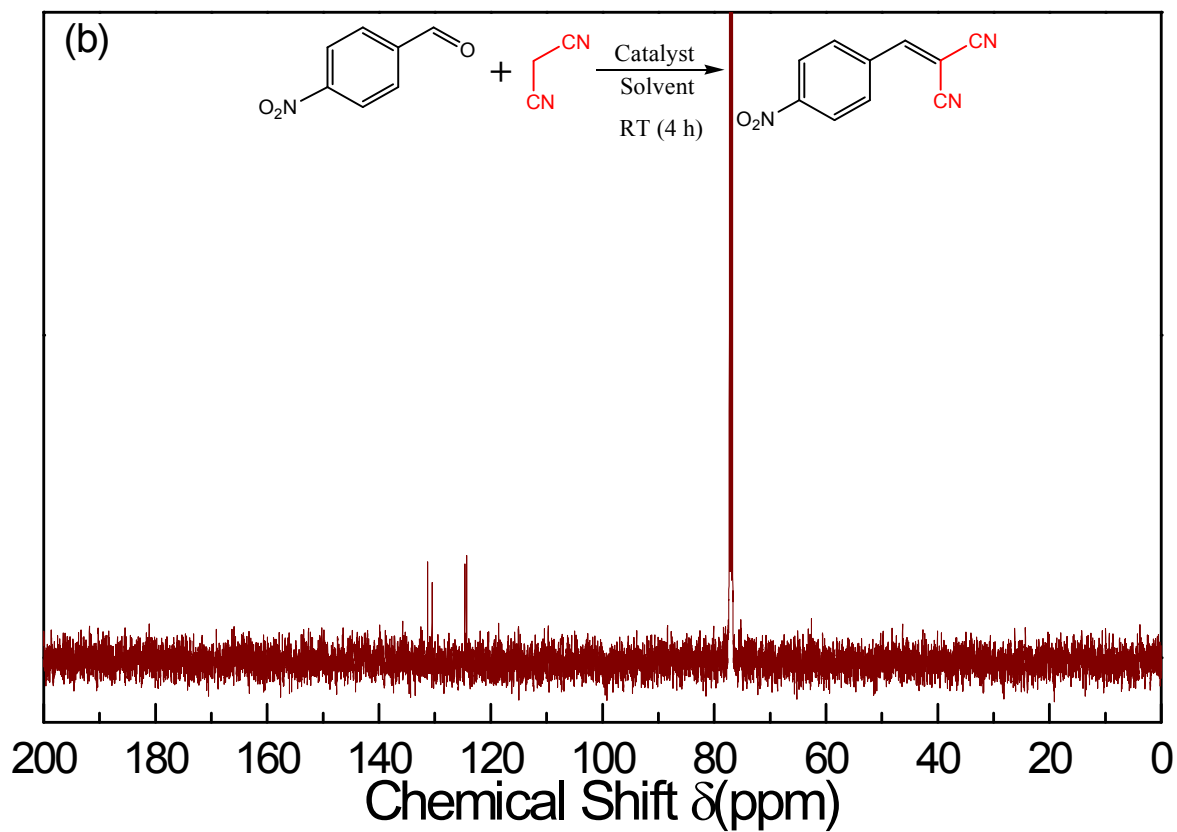
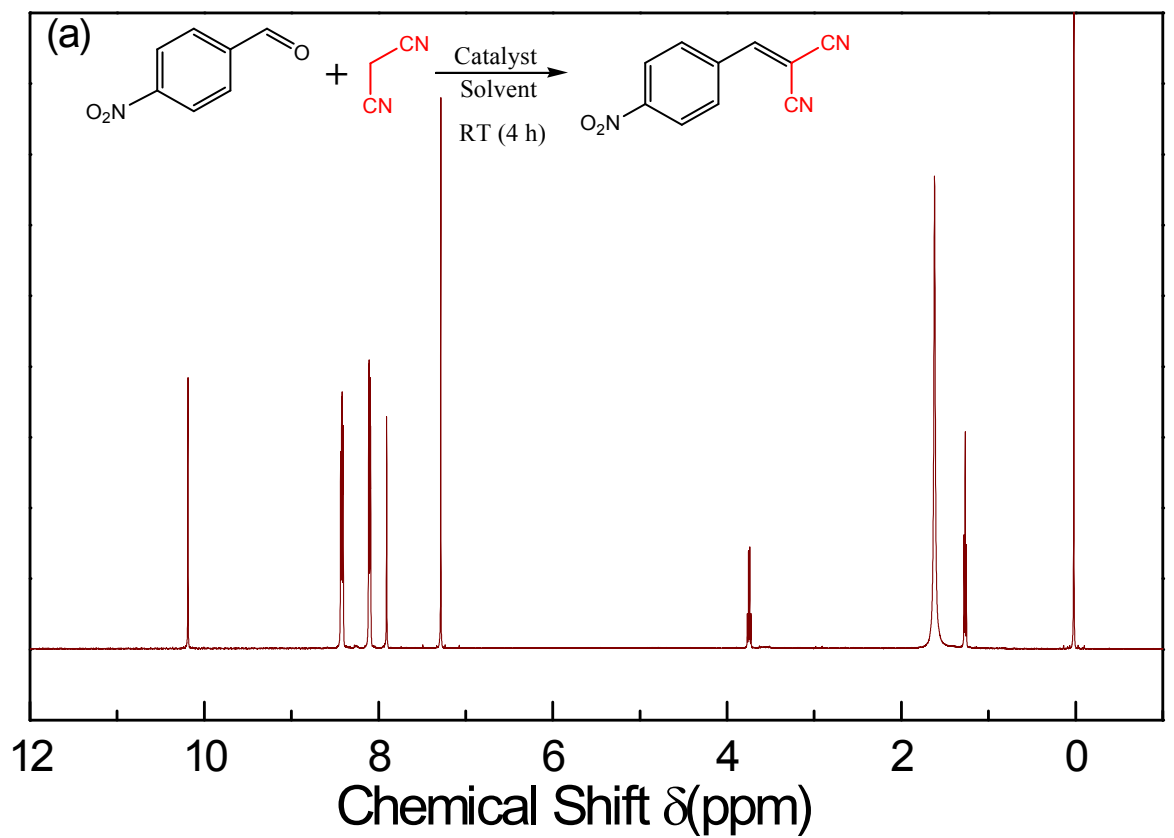


Fig. S33. (a) ^1H and (b) ^{13}C NMR spectra of 4-Nitro benzylidene malononitrile.

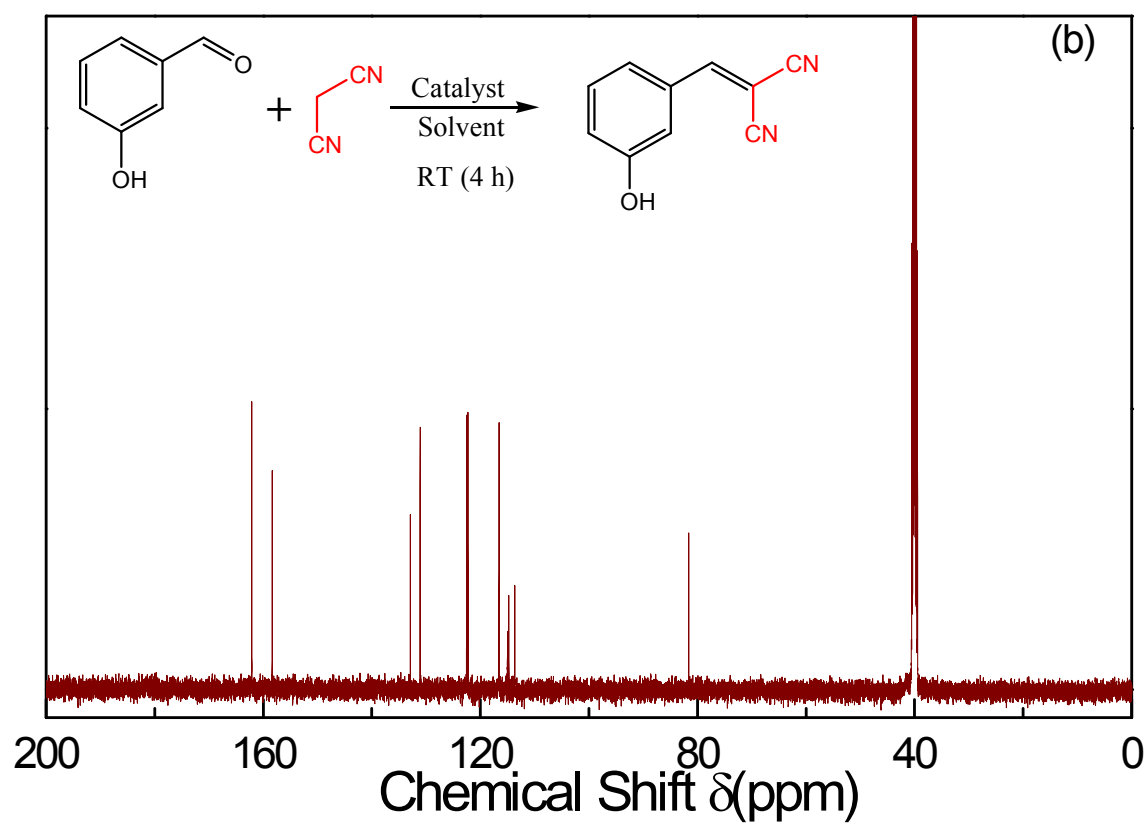
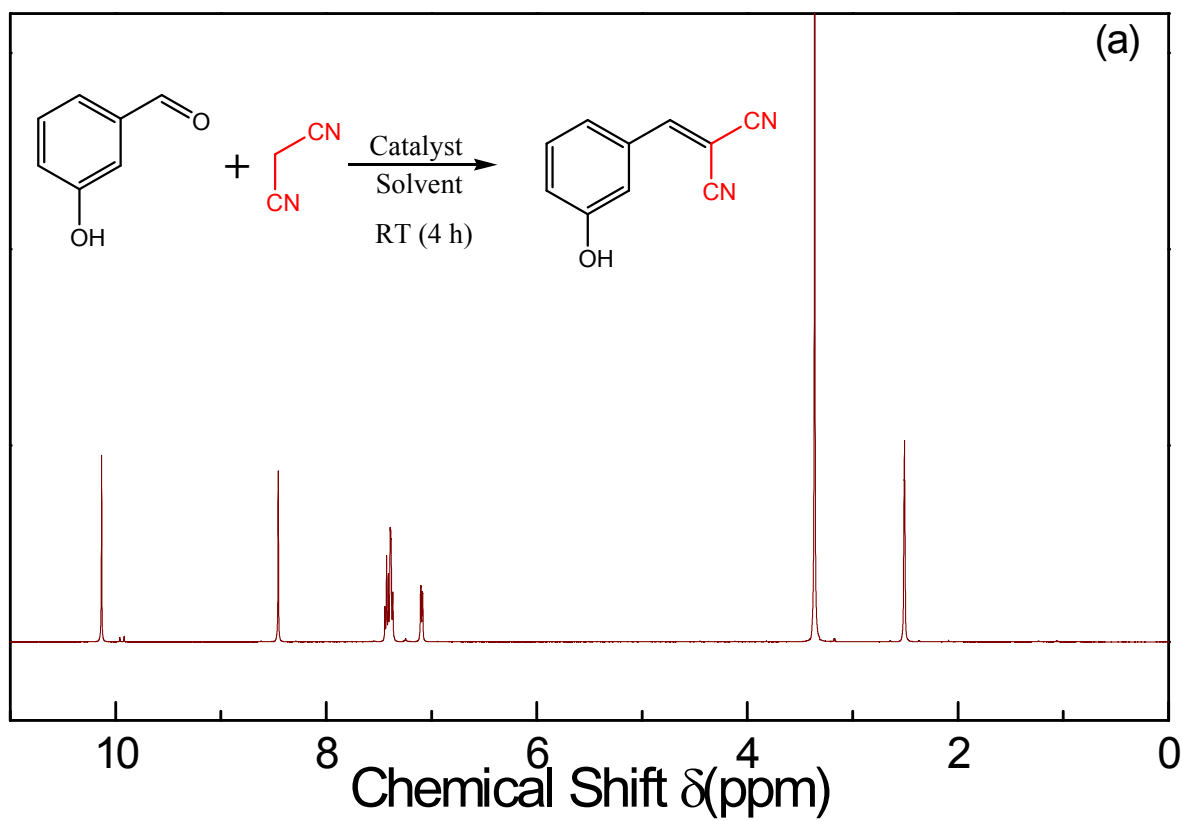


Fig. S34. (a) ^1H and (b) ^{13}C NMR spectra of 3-hydroxy benzylidinemalononitrile.

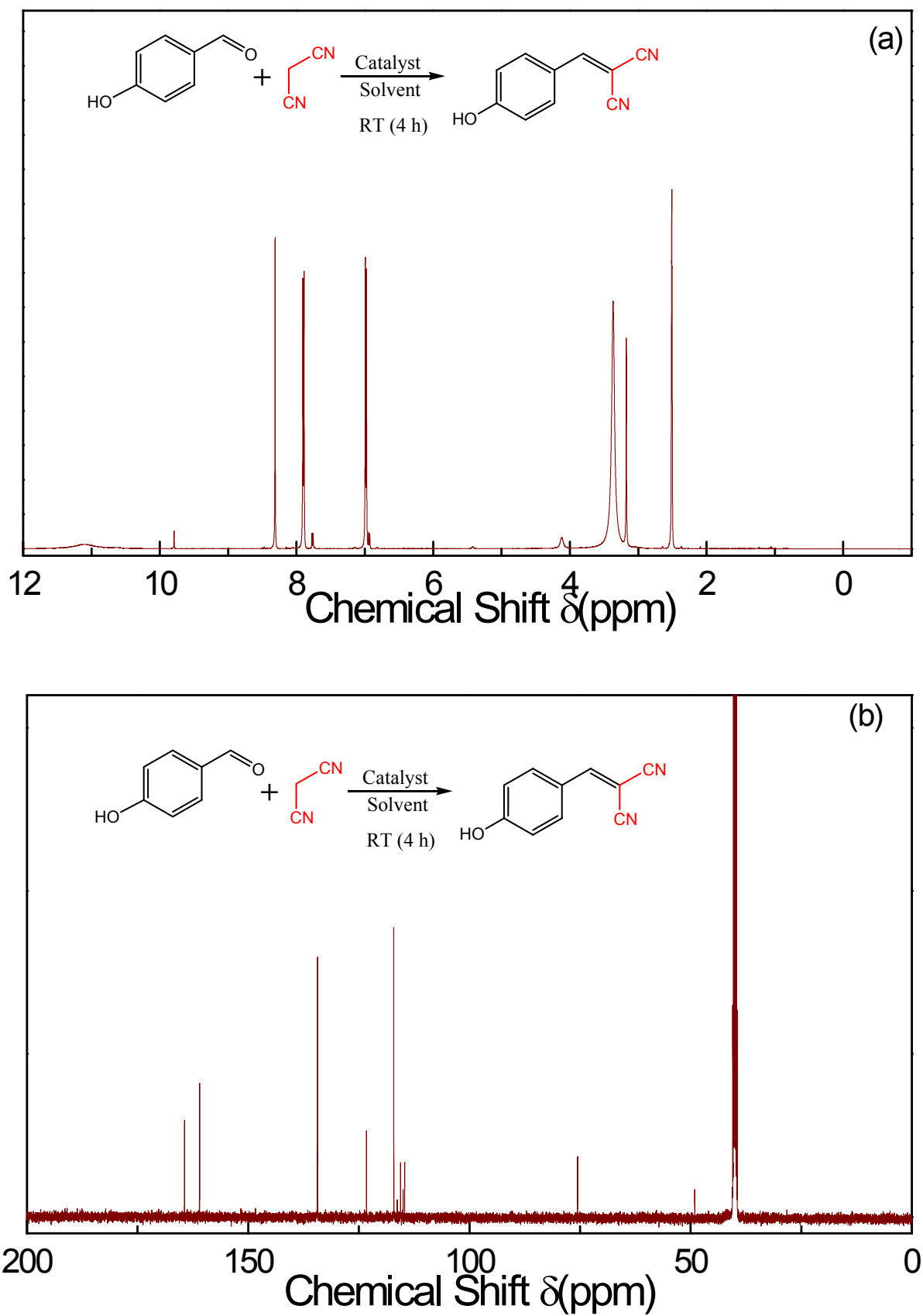


Fig. S35. (a) ¹H and (b) ¹³C NMR spectra of 4-hydroxy benzylidinemalononitrile.

References:

1. A. Anderson, T. Goetzen, S. A. Shackelford and S. Tsank, *Syn. Commun.*, 2000, **30**, 3227-3232.
2. (a) M. Chaudhary, A. K. Nayak, R. Muhammad, D. Pradhan and P. Mohanty, *ACS Sustainable Chem. Eng.*, 2018, **6**, 5895-5902. (b) R. Muhammad, P. Rekha and P. Mohanty, *RSC Adv.*, 2016, **6**, 17100-17105.
3. L. Shao, Y. Li, J. Huang and Y. -N. Liu, *Ind. Eng. Chem. Res.*, 2018, **57**, 2856-2865.
4. S. Ren, M. J. Bojdys, R. Dawson, A. Laybourn, Y. Z. Khimiyak, D. J. Adams, and A. I. Cooper, *Adv.Mater.*, 2012, **24**, 2357-2361.
5. L. Stegbauer, K. Schwinghammer and B. V. Lotsch, *Chem. Sci.*, 2014, **5**, 2789-2793.
6. W. -C. Song, X. -K. Xu, Q. Chen, Z. -Z. Zhuang and X. -H. Bu, *Polym. Chem.*, 2013, **4**, 4690-4696.
7. Y. H. Abdelmoaty, T. D. Tessema, F. A. Choudhury, O. M. El-Kadri and H. M. El-Kaderi, *ACS Appl. Mater. Interfaces*, 2018, **10**, 16049-16058.
8. P. Puthiaraj, S. S. Kim and W. S. Ahn, *Chem. Engg., J.*, 2016, **283**, 184-192.
9. X. Zhu, S. M. Mahurin, S. An, C. Do-Thanh, C. Tian, Y. Li, L. W. Gill, E. W. Hagaman, Z. Bian, J. Zhou, J. Hu, H. Liu and S. Dai, *Chem. Commun.*, 2014, **50**, 7933-7936.
10. W. Wang, Y. Yuan, F. Sun and G. Zhu, *Chin. Chem. Lett.*, 2014, **25**, 1407-1410.
11. R. Xue, H. Guo, L. Yue, T. Wang, M. Wang, Q. Li, H. Liu and W. Yang, *New J. Chem.*, 2018, **42**, 13726-13731.
12. H. A. Patel, F. Karadas, A. Canlier, J. Park, E. Deniz, Y. Jung, M. Atilhan and C. T. Yavuz, *J. Mater. Chem.*, 2012, **22**, 8431-8437.
13. S. Zulfiqar, M. I. Sarwar and C. T. Yavuz, *RSC Adv.*, 2014, **4**, 52263-52269.
14. (a) A. Azzouz, A.V. Ursu, D. Nistor, T. Sajin, E. Assaad and R. Roy, *Thermochim. Acta*, 2009, **496**, 45-49. (b) D.-H. Lan, F.-M. Yang, S.-L. Luo, C.-T. Au and S.-F. Yin, *Carbon*, 2014, **73**, 351-360. (c) J. I. D. Cosimo, V. K. D'iez, M. Xu, E. Iglesia and C. R. Apestegu'ia, *J. Catal.*, 1998, **178**, 499-510. (d) S. Sankaranarayanan, C. A. Antonyraj and S. Kannan, *Bioresour. Technol.*, 2012, **109**, 57-62. (e) S. Verma, G. Kumar, A. Ansari, R. I. Kureshy and N.-U. H. Khan, *Sustain. Energy Fuels*, 2017, **1**, 1620-1629.
15. M. J. Frisch, G. W. Trucks, H. B. Schlegel et al. The Gaussian reference is GAUSSIAN 09 (Revision A.02), Gaussian, Inc., Wallingford, CT, 2016.